Palaeogeography, Palaeoclimatology, Palaeoecology 561 (2021) 110037

Contents lists available at ScienceDirect

Palaeogeography, Palaeoclimatology, Palaeoecology

journal homepage: www.elsevier.com/locate/palaeo

Invited Research Papers

Coral-based proxy calibrations constrain ENSO-driven sea surface temperature and salinity gradients in the Western Pacific Warm Pool

Ahmad T. Mohtar[a,b,*], Konrad A. Hughen[c,1], Nathalie F. Goodkin[a,b,d,1], Iulia-Madalina Streanga[c], Riovie D. Ramos[e], Dhrubajyoti Samanta[a], James Cervino[c,f], Adam D. Switzer[a,b]

[a] Asian School of the Environment, Nanyang Technological University, Singapore
[b] Earth Observatory of Singapore, Nanyang Technological University, Singapore
[c] Marine Chemistry and Geochemistry, Woods Hole Oceanographic Institution, United States
[d] Department of Earth and Planetary Sciences, American Museum of Natural History, United States
[e] Department of Environmental Sciences, William Paterson University, United States
[f] Restoration and Conservation Advisement, United States

ARTICLE INFO

Keywords:
Sr/Ca
$\delta^{18}O_{sw}$
Porites spp.
ENSO
Spatial index
Multi-timescale calibration

ABSTRACT

Constraining past variability in ocean conditions in the Western Pacific Warm Pool (WPWP) and examining how it has been influenced by the El-Niño Southern Oscillation (ENSO) is critical to predicting how these systems may change in the future. To characterize the spatiotemporal variability of the WPWP and ENSO during the past three decades, we analyzed climate proxies using coral cores sampled from *Porites* spp. from Kosrae Island (KOS) and Woleai Atoll (WOL) in the Federated States of Micronesia. Coral skeleton samples drilled along the major growth axis were analyzed for oxygen isotopes ($\delta^{18}O_c$) and trace element ratios (Sr/Ca), used to reconstruct sea surface salinity and temperature (SSS and SST). Pseudocoral $\delta^{18}O$ time series ($\delta^{18}O_{pseudo}$) were calculated from gridded instrumental observations and compared to $\delta^{18}O_c$, followed by fine-tuning using coral Sr/Ca and gridded SST, to produce age models for each coral. The thermal component of $\delta^{18}O_c$ was removed using Sr/Ca for SST, to derive $\delta^{18}O$ of seawater ($\delta^{18}O_{sw}$), a proxy for SSS. The Sr/Ca, and $\delta^{18}O_{sw}$ records were compared to instrumental SST and SSS to test their fidelity as regional climate recorders. We found both sites display significant Sr/Ca-SST calibrations at monthly and interannual (dry season, wet season, mean annual) timescales. At each site, $\delta^{18}O_{sw}$ also exhibited significant calibrations to SSS across the same timescales. The difference between normalized dry season SST (Sr/Ca) anomalies from KOS and WOL generates a zonal SST gradient ($KOSWOL_{SST}$), capturing the east-west WPWP migration observed during ENSO events. Similarly, the average of normalized dry season $\delta^{18}O_{sw}$ anomalies from both sites produces an SSS index ($KOSWOL_{SSS}$) reflecting the regional hydrological changes. Both proxy indices, $KOSWOL_{SST}$ and $KOSWOL_{SSS}$, are significantly correlated to regional ENSO indices. These calibration results highlight the potential for extending the climate record, revealing spatial hydrological gradients within the WPWP and ENSO variability back to the end of the Little Ice Age.

1. Introduction

El Niño-Southern Oscillation (ENSO) is the most dominant coupled mode of tropical climate variability that is known to affect global climate through teleconnections (Bjerknes, 1969; Rasmusson and Carpenter, 1982; Cane, 1986; Philander, 1990; Trenberth, 1997; Wallace et al., 1998; Thompson et al., 2006; Santoso et al., 2017; Timmermann et al., 2018). Changes in intensity and frequency of ENSO events (i.e. El Niño and La Niña) are known to cause extreme weather conditions (McPhaden et al., 2006), impacting human health (McKibben et al., 2017; Anyamba et al., 2019; Lam et al., 2019), infrastructure (Brakenridge et al., 2017; Giuliani et al., 2019) and food security (Williams and Funk, 2011; Anderson et al., 2019). However, the predictability of ENSO events remains challenging due in part to our incomplete knowledge of the full range of spatiotemporal natural behavior of ENSO (Lu et al., 2018). Our limited understanding of long

* Corresponding author at: Asian School of the Environment, Nanyang Technological University, Singapore.
E-mail addresses: A160107@e.ntu.edu.sg (A.T. Mohtar), khughen@whoi.edu (K.A. Hughen), ngoodkin@amnh.org (N.F. Goodkin), istreanga@whoi.edu (I.-M. Streanga), ramosr34@wpunj.edu (R.D. Ramos), dhruba@ntu.edu.sg (D. Samanta), jcervino@whoi.edu (J. Cervino), aswitzer@ntu.edu.sg (A.D. Switzer).
[1] These authors contributed equally to manuscript preparation.

https://doi.org/10.1016/j.palaeo.2020.110037
Received 8 June 2020; Received in revised form 17 September 2020; Accepted 19 September 2020
Available online 01 October 2020

term-ENSO variability stems from the short duration of instrumental records. To fill this gap, numerous paleoclimate studies have reconstructed ENSO variability over the past centuries and millennia, based on corals (Cole et al., 1993; Tudhope et al., 2001; Cobb et al., 2003; Cobb et al., 2013; Emile-Geay et al., 2013; McGregor et al., 2013; Grothe et al., 2020), sediments (Conroy et al., 2008; Koutavas and Joanides, 2012; Thirumalai et al., 2013; Barr et al., 2019), tree rings (Cook et al., 2003; Cook et al., 2006; D'Arrigo et al., 2006; Li et al., 2011; Schollaen et al., 2015) and speleothems (Brook et al., 1999; Lachniet et al., 2004; Chen et al., 2016; Sun et al., 2018; Zhao et al., 2019). However, many ENSO reconstructions show disagreement during the preindustrial period (McGregor et al., 2009; Emile-Geay et al., 2013) and long-term ENSO variability may appear differently depending on location in the eastern, central or western Pacific (Li et al., 2011; Nurhati et al., 2011; Partin et al., 2013; Yamoah et al., 2016; Shi and Wang, 2019). Some studies rely on teleconnections to distant regions (Moy et al., 2002; Schöngart et al., 2004; D'Arrigo et al., 2005; Räsänen et al., 2016; Stahle et al., 2016), whereas Pacific corals provide high-resolution records of hydrographic variability within ENSO's spatial footprint. However, only a limited number of studies in the Western Pacific Warm Pool (WPWP) extend beyond 100–200 years to constrain long-term ENSO variability (e.g.,(Tudhope et al., 1995; McGregor and Gagan, 2004; Linsley et al., 2006; Quinn et al., 2006; Gorman et al., 2012; Osborne et al., 2014), a key region concerning the Walker Circulation and ENSO. Our limited knowledge of spatio-temporal ENSO behavior over long timescales results in significant uncertainties in modelling ENSO within general circulation models (GCMs) (Wittenberg, 2009; Schmidt et al., 2011; Newman et al., 2018). These challenges in modelling ENSO are exacerbated by the mean-state model biases such as, westward extended sea surface temperature (SST) variability and double Inter Tropical Convergence Zone (ITCZ) in the state-of-the-art GCMs over WPWP (Samanta et al., 2018; Samanta et al., 2019).

The WPWP, defined as the region with mean annual SST above 28 °C typically between 15S°-15°N, 120°E-160°W, forms when the trade winds transport warm water across the tropical Pacific to the western boundary formed by the Maritime Continent (Wyrtki, 1974; Enfield et al., 2006). The WPWP then feeds the western boundary currents delivering heat from the tropics to the sub-tropics via the Kuroshio and East Australia Currents (Hu et al., 2015; Todd et al., 2019). During a La Niña event, the WPWP is anomalously warm and rainfall increases, and the opposite occurs in an El Niño event (Bjerknes, 1966; Wyrtki, 1974; McPhaden, 1999). During El Niño, longitudinal gradients of SST and sea surface salinity (SSS) anomalies form as the weaker trade winds deliver “less-warm” and saltier water to the WPWP (McPhaden and Picaut, 1990; Picaut et al., 1996; Delcroix and McPhaden, 2002; McPhaden, 2018). Recent studies have also shown differences in the spatial SST and SSS signatures of “central” versus “eastern” types of El Niño events (Singh et al., 2011; Capotondi et al., 2015; Qi et al., 2019). Changes in the WPWP are therefore reflective of the intensity and location of ENSO events and provide an ideal opportunity to study past ENSO variability (Wang and Liu, 2016; Hu et al., 2017; Kidwell et al., 2017). Unfortunately, the sparsity and short temporal length of climate records in this region have prevented us from understanding past warm pool zonal migrations at decadal to centennial timescales (Cravatte et al., 2009). Paleoclimate records from across this region would allow studying the extension of WPWP reconstructions and provide a more holistic understanding of WPWP and ENSO variability back through time.

Paleoclimate reconstructions from fast-growing, long-lived corals are valuable for extending the tropical instrumental record, including ENSO, beyond the onset of the industrial revolution in the late 1800s (Quinn et al., 1996; Alibert and McCulloch, 1997; Zinke et al., 2005; Mitsuguchi et al., 2008). The ratio of stable oxygen isotopes ($^{18}O/^{16}O$, reported as $\delta^{18}O$ relative to a standard) in corals is commonly used as a combined proxy of SST and SSS (Epstein et al., 1953). During calcification, coral $\delta^{18}O$ ($\delta^{18}O_c$) varies in response to both the temperature and seawater $\delta^{18}O$ composition ($\delta^{18}O_{sw}$) of the water surrounding the coral colony. Generally, $\delta^{18}O_{sw}$ has a linear relationship with SSS (Urey, 1947). Also, corals incorporate relatively less Sr into their calcium carbonate ($CaCO_3$) skeleton with increasing temperatures, therefore resulting in an inverse correlation between Sr/Ca ratios and SST (Smith et al., 1979). Sr/Ca is insensitive to changes in SSS and is therefore commonly used to reconstruct SST (Beck et al., 1992; Alibert and McCulloch, 1997; Heiss et al., 1997; Gagan et al., 1998; Hughen et al., 1999; Corrège et al., 2000; Linsley et al., 2000; Hendy et al., 2002; Fallon et al., 2003; Felis et al., 2004; Linsley et al., 2004; Stephans et al., 2004; Goodkin et al., 2005; Quinn et al., 2006; DeLong et al., 2007; Pfeiffer et al., 2009; DeLong et al., 2011; DeLong et al., 2012; Wu et al., 2013; Bolton et al., 2014; Sagar et al., 2016; Ramos et al., 2017). Due to its fidelity as a proxy for SST, Sr/Ca is frequently used to remove the temperature signal from coral $\delta^{18}O_c$. Through coupled Sr/Ca and $\delta^{18}O$ measurements, Sr/Ca-predicted SST is subtracted from the $\delta^{18}O_c$ signal to derive a record of residual sea water $\delta^{18}O$, or $\delta^{18}O_{sw}$ (McCulloch et al., 1994; Gagan et al., 1998; Ren et al., 2003; Cahyarini et al., 2008). The resulting $\delta^{18}O_{sw}$ record can then be used to reconstruct past changes in surface hydrology (precipitation-evaporation as well as advection) over the past decades to centuries (Corrège et al., 2004; Linsley et al., 2004; Bolton et al., 2014; Hennekam et al., 2018; Pfeiffer et al., 2019).

The long-lived coral genus *Porites* spp. are common in the Indo-Pacific and known for preserving reliable paleoclimate information. Although some factors (e.g., changes in coral vital effects or Sr/Ca of sea water) have been identified as possible sources of non-temperature influences on the coral Sr/Ca paleothermometer (e.g., (de Villiers et al., 1995; Shen et al., 1996; de Villiers, 1999; Cohen et al., 2001; Cohen et al., 2002; Allison and Finch, 2004; Alibert and Kinsley, 2008; Grove et al., 2013; Alpert et al., 2016; Kuffner et al., 2017), many studies have shown success in accurately reconstructing SST from coral Sr/Ca (McCulloch et al., 1994; Marshall and McCulloch, 2001; Goodkin et al., 2005; DeLong et al., 2007; Goodkin et al., 2007; Cahyarini et al., 2009; Pfeiffer et al., 2009; DeLong et al., 2011; DeLong et al., 2013; Wu et al., 2013; Bolton et al., 2014; Ramos et al., 2017; Pfeiffer et al., 2019). Also, a recent study investigating variability in Sr/Ca-SST calibrations across large SST gradients showed that the Sr/Ca-SST slopes do not change randomly but vary systematically with mean SST (Murty et al., 2018). While *Porites* are typically fast-growing corals with minimal growth impacts, calibrating Sr/Ca from each colony against recent instrumental SST is still required to accurately reconstruct SST back in time. Similarly, $\delta^{18}O_c$ may also experience different sensitivities to SST and SSS, given $\delta^{18}O_{sw}$ range of variability may be significant relative to SST (Tudhope et al., 2001; Linsley et al., 2004; Russon et al., 2013) in the context of resultant $\delta^{18}O$ variability. Within the eastern and central tropical Pacific, $\delta^{18}O_c$ tracks variations in ENSO driven mostly by changes to SST (Dunbar et al., 1994; Cobb et al., 2003; Nurhati et al., 2011), whereas central to western Pacific $\delta^{18}O_c$ tracks ENSO through changes in SST and rainfall (Cole et al., 1993; Tudhope et al., 2001; Quinn et al., 2006; Carilli et al., 2014). Recent in-situ seawater $\delta^{18}O$-SSS studies suggest a trend of increasing sensitivities from the eastern to western Pacific, implying differences in the spatial seawater $\delta^{18}O$-SSS relationship (Conroy et al., 2014; Conroy et al., 2017). These findings are coherent with modelling studies, which show significant uncertainties in reconstructing $\delta^{18}O_c$ values due to variable $\delta^{18}O_{sw}$ impacted by ENSO (Liu et al., 2014; Stevenson et al., 2015). Careful, site-specific calibrations of $\delta^{18}O_c$ to instrumental SST and SSS data are therefore also required for each colony.

Our study examines two corals from either side of the heart of the WPWP that capture the longitudinal seesaw of SST and SSS anomalies during ENSO events. We investigate calibrations between coral proxies (Sr/Ca and $\delta^{18}O$) and instrumental SST and SSS, at multiple timescales (monthly, interannual). Additionally, to quantify potential sensitivity of the WPWP to ENSO variability, coral-based zonal SST and SSS gradients

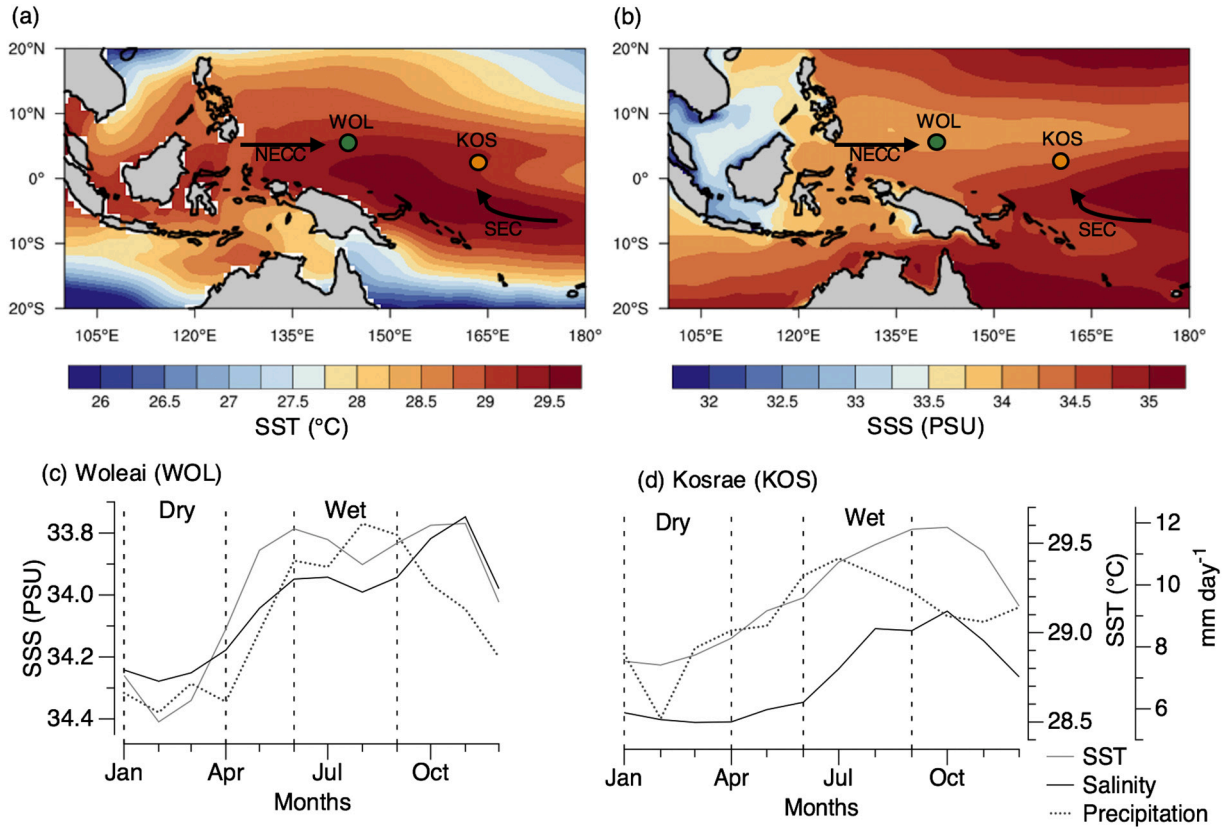

Fig. 1. Study region including Woleai Atoll (WOL; green circle) and Kosrae Island (KOS; orange circle) within the WPWP including a) annual average SST (°C) from 1982 to 2012 from NOAA OISST v2, and b) annual average SSS (psu) from 1982 to 2012 from SODA v3.3.1. Solid arrows indicate the westward and eastward-moving South Equatorial Current (SEC) and North Equatorial Countercurrent (NECC), respectively. Climatologies of SST, SSS, and precipitation from 1982 to 2012 for each site shows c) WOL (centered on 7.5°N, 143.5°E) d) and KOS (grid box centered on 5.5°N, 162.5°E). SST monthly averages are from NOAA OISST v2 (gray) (Reynolds et al., 2002). SSS monthly averages are from SODA v3.3.1 (black) (Carton et al., 2016), and precipitation from CAMSOPI (black dotted) Janowiak and Xie, 1999. Vertical lines designate dry, cool (JFMA) and wet, warm (JJAS) months inferred from rainfall and SST. (For interpretation of the references to colour in this figure legend, the reader is referred to the web version of this article.)

between the two sites are examined for correlations to instrumental ENSO indices. Such spatial information captured in these corals would provide valuable new constraints on not just intensity but type ("eastern" versus "central") of ENSO events.

2. Materials and methods

2.1. Region of study

The islands of the Federated States of Micronesia (FSM) are spread near the equator within the WPWP, characterized by warm mean annual SSTs (> 28 °C) (Wyrtki, 1989) and heavy rainfall inducing SSS below 35 practical salinity units (psu) (Carton et al., 2016). Woleai Atoll (7° 21′ 59.99″ N, 143°53′ 59.99″ E, WOL) and Kosrae Island (5° 18′ 60.00″ N, 162° 58′ 59.99″ E, KOS) are located near the eastern edge of the WPWP (Fig. 1) and show independent seasonal variability dependent on the meridional movement of the warm pool (Yan et al., 1992). Both sites capture seasonal SST variability, displaying maxima during wet season (July-September) (~29.5 °C) and dry season (January-April) (~28.5 °C) ((Reynolds et al., 2002); Fig. 1c, d).

The WPWP exhibits a salinity front (isohaline ~34.6 psu) between the warm-fresh waters of the North Equatorial Counter Current and less warm-saltier waters of the South Equatorial Current (Fig. 1a, b) (Delcroix and Henin, 1991; Picaut et al., 1996; Hu et al., 2015). Salinity fronts are also observed at the boundaries of the Inter Tropical Convergence Zone (ITCZ), as seawater salinity increases with decreasing precipitation (Eldin et al., 2004; Kao and Lagerloef, 2015) (Fig. 1b; 34.5–35 salinity band). The salinity front is closest to Kosrae Island (~34.4 psu) and Woleai Atoll (~34.2 psu) during the dry season when both the warm pool and ITCZ migrate to their southernmost extent (Delcroix and Henin, 1991; Carton et al., 2016). During this period, both sites' SSS maxima coincide with the mean precipitation and SST minima observed from a 30-year seasonal climatology (Fig. 1c, d).

At interannual timescales, the salinity front and the eastern edge of the WPWP are subject to zonal migrations of up to several thousands of kilometers, eastward and westward during mature phases of El Niño and La Niña, respectively (Picaut et al., 1996; Delcroix, 1998; Maes et al., 2004). The January to April (JFMA) SSS and SST anomalies for El Niño and La Niña events reveal that Woleai Atoll and Kosrae Island experience opposite changes reflective of the extent of zonal migration of the WPWP influenced by ENSO (Fig. 2). These opposite relationships provide a distinct spatial signature of ENSO variability that can be distinguished from background trends (e.g., regional or global warming), and record changes due to the type ("eastern" versus "central") as well as the intensity of ENSO events.

2.2. Coral collection, sampling, and analysis

Porites spp. coral cores from two separate regions of the FSM were drilled during the R/V *Alucia* Micronesia expedition in October 2012. Both coral cores were taken along the colony growth axis using an underwater hydraulic drill. The first coral core, measuring 4.6 m long, was sampled adjacent to the southern islet of WOL (7.4°N, 144°E) close to one of several entrances where open ocean waters flush the lagoon. The second coral core, measuring 3.5 m long, was retrieved off the southern coast of KOS (5.3°N, 163°E) and was directly exposed to open-

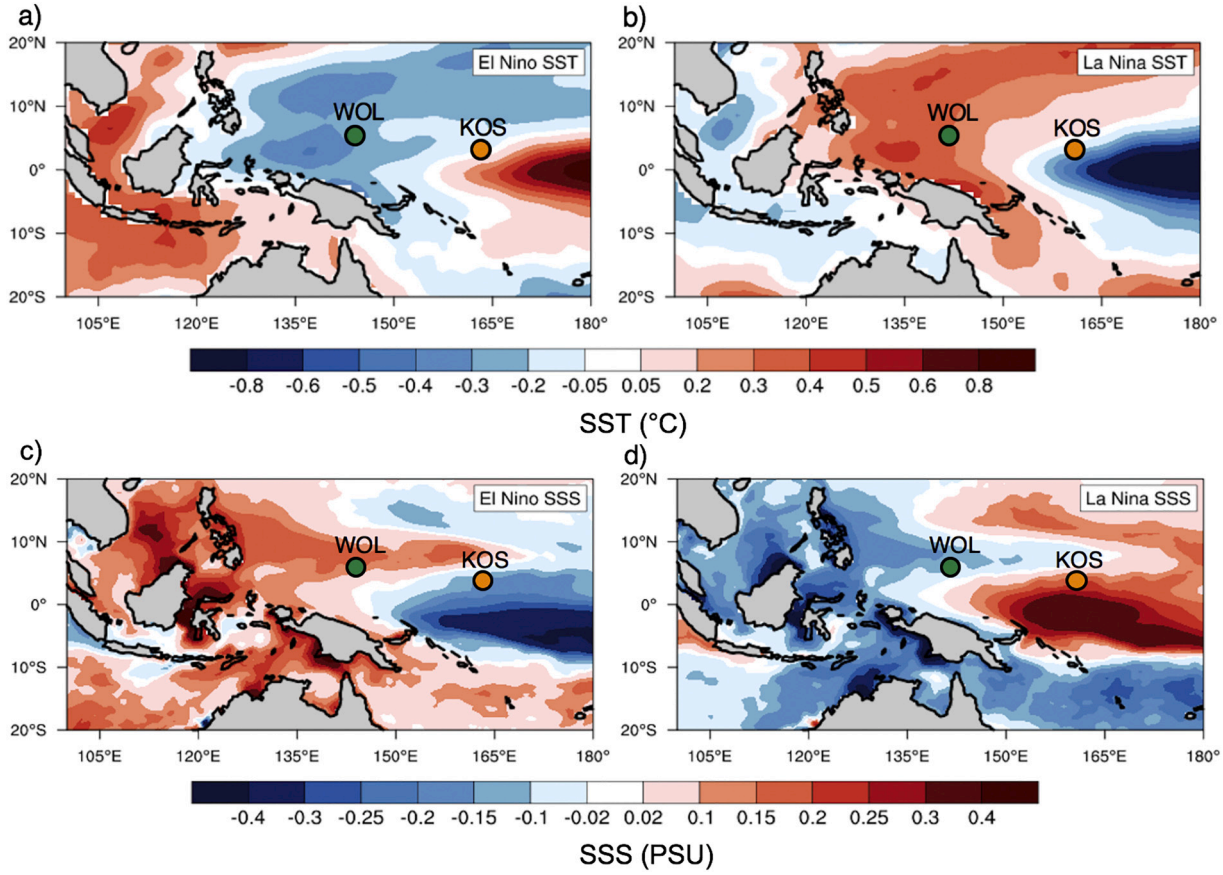

Fig. 2. Composite dry season (JFMA averaged) anomaly of SST (in ˚C) and SSS (in psu) during El Niño (1982, 1986, 1987, 1991, 1994, 1997, 2002, 2004, 2006, 2009) and La Niña (1983, 1984, 1988, 1995, 1998, 1999, 2000, 2005, 2007, 2008, 2010, 2011) years. SSTs for (a) El Niño, (b) La Niña, and SSSs for (c) El Niño (d) La Niña following Niño 4 index. Coral sites are indicated by green and yellow circles. (For interpretation of the references to colour in this figure legend, the reader is referred to the web version of this article.)

ocean waters. Unlike WOL, KOS may experience land-sea thermal gradients due to larger landmass compared to smaller islets of WOL.

Five-millimeter slabs were cut from the cores with a diamond-blade rock saw at Woods Hole Oceanographic Institution (WHOI). Each slab was soaked in bleach, rinsed and subsequently ultrasonicated in deionized water for 15 min and dried for 48 h in a 50 ˚C oven. Slabs were then x-rayed at the Diagnostic Imaging Laboratory at the National University Hospital Singapore at 50 kV, 10 mA, 500 ms, and a focal point of 100 cm. The x-ray positives allow for the visualizing of annual density bands and delineating sampling paths parallel to the extending corallites (Fig. 3, Fig. S2). Infrequent skeletal anomalies can be seen in the x-rays and slab surfaces, and sampling tracks are selected to avoid any such anomalies. In addition, skeletal density was determined along the sampling track based on calibrated optical density in the x-radiographs (Carricart-Ganivet and Barnes, 2007). We found no systematic changes in mean skeletal density along the sample track, indicating no addition of secondary aragonite (Hendy et al., 2007) (Fig. S1).

The top 47 cm of KOS and 30 cm of WOL coral slabs were sampled at 0.5 mm intervals using a manual drill press fitted with a one mm drill bit. The sampling path was consistently drilled to one mm depth, generating approximately 250–350 μg of coral powder. The powder samples were split to allocate 50–80 μg for stable oxygen isotope analysis and the remainder for trace element analysis.

Stable isotope analysis was conducted on a Thermo Fisher MAT-253 Isotope Ratio Mass Spectrometer (IRMS) coupled to a Kiel IV Kiel Carbonate Device at the Asian School of the Environment (ASE) to generate the WOL and KOS $\delta^{18}O$ records. Isotopic measurements were calibrated relative to Vienna Peedee belemnite (VPDB) using Natural Bureau of Standards (NBS)-19 (−2.20‰) (Stichler, 1995) with further linear calibration to a range of standards with NBS-18 at a minimum ($\delta^{18}O_{VPDB}$ = −23‰). Carbonate standards (Carrara, TSF and Estremoz) were repeatedly measured yielding average values of −1.964‰ (± 0.06‰, N = 2195), −2.254‰ (± 0.07‰, N = 1649) and − 5.972 (± 0.07‰, N = 2006), respectively.

Sr/Ca of WOL slabs were analyzed at ASE, and Sr/Ca of KOS was analyzed at WHOI; both on Thermo I-Cap Inductively Coupled Optical Emission Spectrometers (ICP-OES). Powder samples were digested with 2.5 ml of 5% HNO_3 in an 8 ml tube, vortexed for 30 s and left to homogenize overnight. A reference solution was measured between every sample to correct for instrumental drift, and calibration standards were routinely analyzed to correct for matrix effects as a result of variable calcium concentration (Schrag, 1999). Analytical precision and accuracy were monitored by measuring reference standard JCp-1 (Okai et al., 2002) and an in-house standard Bunaken. The reproducibility of JCp-1 at ASE is 0.18% (average 8.824 ± 0.018 mmol/mol, n = 1146) and at WHOI is 0.10% (average 8.828 ± 0.009 mmol/mol, n = 124), consistent with interlaboratory values (8.838 ± 0.089 mmol/mol) (Hathorne et al., 2013). Bunaken standards measured at WHOI were also within uncertainties of ASE (8.838 ± 0.014 mmol/mol n = 971, 8.819 ± 0.023 mmol/mol, n = 432; average and number of observations at WHOI and ASE respectively).

2.3. Climate data sources to build coral age model

Gridded instrumental and reanalysis products were utilized to build coral age model. For SSS, monthly resolved gridded 0.25° × 0.25° Simple Ocean Data Assimilation / Sea Ice Reanalysis v3 (SODA) (Carton et al., 2016) data centered at 7.25°N, 143.75°E (Woleai Atoll) and

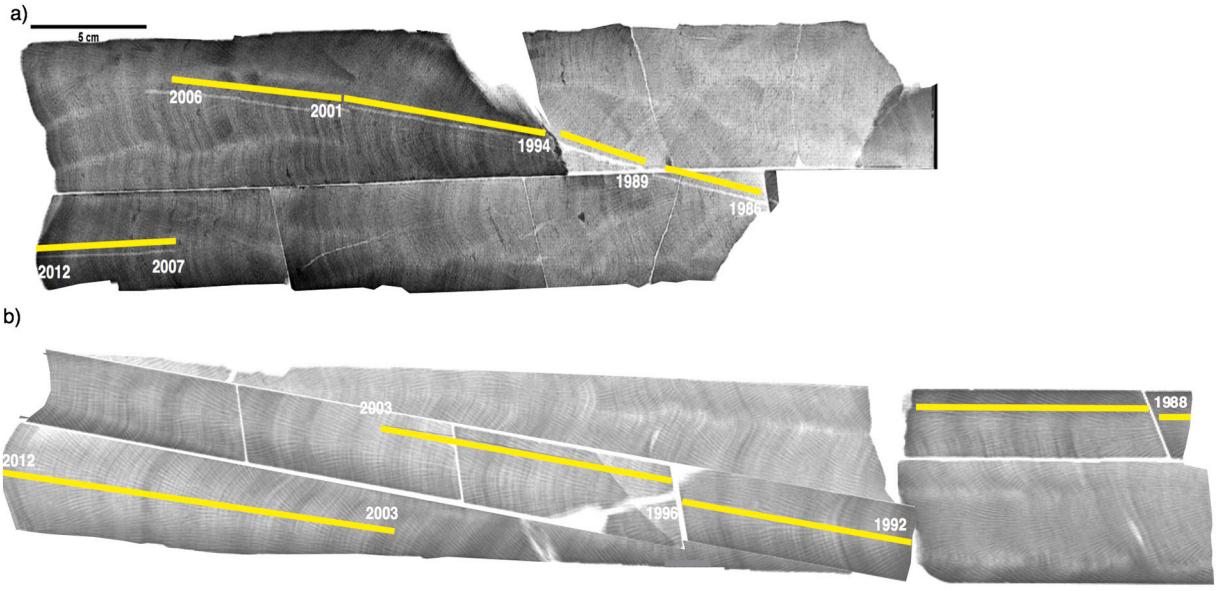

Fig. 3. X-ray positive images of corals for (a) Woleai (WOL), and (b) Kosrae (KOS). Yellow lines denote the sampling path of each coral for geochemical analyses. X-radiographs are contrast enhanced to increase clarity of density banding and both cores are at the same scale shown above. (For interpretation of the references to colour in this figure legend, the reader is referred to the web version of this article.)

5.25°N, 162.75°E (Kosrae Island) were used. For SST, gridded 1° × 1° monthly NOAA Optimum Interpolation SST v2 data (OISST) (Reynolds et al., 2002) centered at 7.5°N, 143.5°E (Woleai Atoll) and 5.5°N,162.5°E (Kosrae Island) were utilized.

2.4. Establishing coral chronologies

The annual chronology of KOS was established by counting annual density bands in coral x-ray images (Fig. 3b), where a light and a dark pair of bands indicate one year. However, this method could not be applied to WOL due to less well-defined banding (Fig. 3a), which may have resulted from sub-optimal corallite orientation due to variable growth directions, microenvironment, or species-specific factors (Knutson et al., 1972; DeLong et al., 2013). To further refine the age models of our corals, we developed pseudo-coral $\delta^{18}O$ records ($\delta^{18}O_{pseudo}$) for the KOS and WOL sites calculated by the known thermodynamic relationships of $\delta^{18}O$ to SST and SSS. First, to calculate seawater $\delta^{18}O$ ($\delta^{18}O_{SW}$), we applied site-centered monthly gridded SODA SSS (1986–2012) to the regionally established $\delta^{18}O_{SW}$-SSS relationship based on an in-situ study from the Western Pacific (Morimoto et al., 2002) (Eq. (1)). Site-centered gridded $\delta^{18}O_{SW}$ and SST data (1986–2012) were then incorporated into the $\delta^{18}O_c$-SST paleothermometer calibration equation derived from (Leclerc and Schmidt, 2001) to generate $\delta^{18}O_{pseudoKOS}$ and $\delta^{18}O_{pseudoWOL}$, representing thermodynamic carbonate values (Thompson et al., 2011) (Eq. (2)). We adopted the intercepts from the original studies as the pseudocoral is only used to assign annual tie points, not convert data.

$$\delta^{18}O_{sw} = 0.4236 \times SSS_{SODA} - 14.244 \quad (1)$$

$$\delta^{18}O_{pseudo} = 0.45 - 0.2 \times SST_{OISSST} + \delta^{18}O_{sw} \quad (2)$$

We performed a 3-step procedure to peak-match coral proxies to gridded climate variables. The first step was to age-assign annual tie points between $\delta^{18}O_{pseudo}$ and $\delta^{18}O_c$ using Analyseries software (Paillard et al., 1996). Enriched (depleted) $\delta^{18}O_c$ was aligned with seasonally enriched (depleted) $\delta^{18}O_{pseudo}$ (Fig. S1). An additional two tie-points were prescribed sub-annually at inflection points between seasonal warm/wet and cool/dry extremes. Second, these tie-points were applied to the corresponding Sr/Ca record and fine-tuned against site-centered SST_{OISSST} data to ensure that Sr/Ca maxima align with SST minima and yield strong correlations. Next, the fine-tuned tie-points were re-applied to the $\delta^{18}O_c$ record for comparison to $\delta^{18}O_{pseudo}$ to ensure peaks and troughs still match, and optimize the relationships between both proxies ($\delta^{18}O_c$, Sr/Ca) and gridded variables ($\delta^{18}O_{pseudo}$, SST). Finally, the age-modelled proxy records ($\delta^{18}O_c$, Sr/Ca) were linearly interpolated to generate records at monthly timescales.

3. Results

3.1. Monthly reconstruction and calibration of SST

Both sites have a similar mean seasonal Sr/Ca range of 0.068 mmol/mol (8.653 to 8.722 mmol/mol) at WOL and 0.073 mmol/mol (8.757 to 8.830 mmol/mol) at KOS. Type (II) Pearson's Major axis linear regressions of monthly Sr/Ca to WOL and KOS SST reveal significant inverse relationship (Fig. 4a):

$$\text{WOL Sr/Ca} = 10.188\ (\pm 0.018) - 0.052\ (\pm 0.003) \times \text{SST}\ (^{\circ}\text{C}) \quad (3)$$

$r = -0.65$, $p < 0.0001$, RMSR = 0.6 °C, $n = 324$, SST range = 2.8 °C, years 1986–2012.

$$\text{KOS Sr/Ca} = 10.861\ (\pm 0.029) - 0.071\ (\pm 0.005) \times \text{SST}\ (^{\circ}\text{C}) \quad (4)$$

r = -0.60, $p < 0.0001$, RMSR = 0.6°C, n = 300, SST range = 2.5°C, years 1988-2012

where root mean squared of the residual (RMSR) measures the average absolute residuals between the instrumental and reconstructed SST.

While both coral sites have relatively similar SST ranges, and monthly Sr/Ca-SST slopes are in agreement with previous studies (Alibert and McCulloch, 1997; Gagan et al., 1998; Marshall and McCulloch, 2002; Quinn and Sampson, 2002; Linsley et al., 2004; Quinn et al., 2006; Wu et al., 2013; Sadler et al., 2016; Brenner et al., 2017), WOL has a shallower slope (-0.052 mmol/mol $C^{\circ -1}$) compared to KOS (-0.071 mmol/mol $C^{\circ -1}$). Coral sub-sampling resolution is high, due to a KOS extension rate of 18.5 mm $year^{-1}$ and WOL of 11 mm $year^{-1}$, providing 37 and 22 samples per year, enough to resolve ~bi-weekly SST changes. Coral extension rates differ between cores, and could potentially account for slope differences through 'biosmoothing' or the infilling of the skeleton with aragonite precipitated in

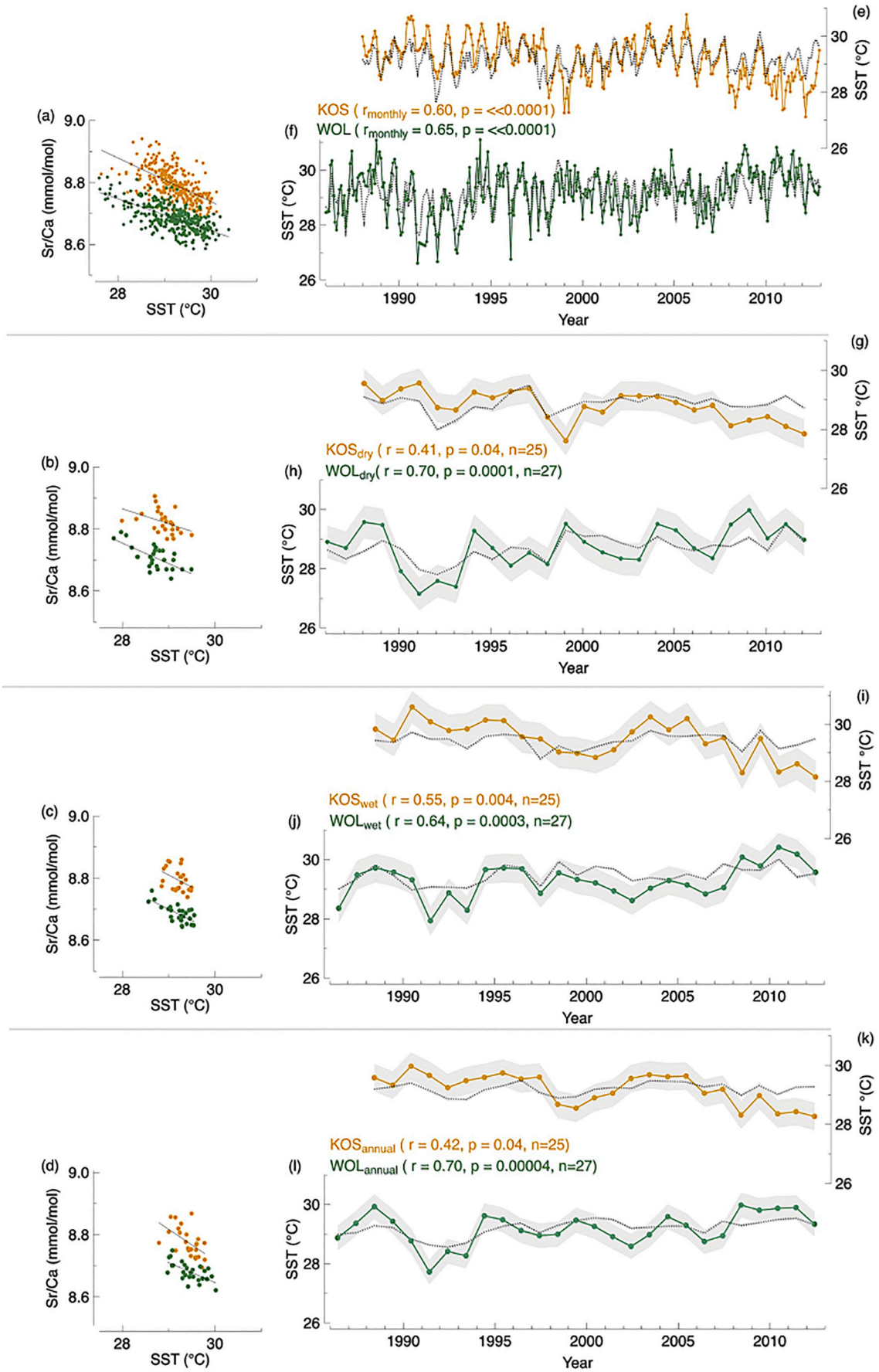

Fig. 4. Sr/Ca (mmol/mol) from KOS (orange) and WOL (green) are inversely and significantly correlated with OISST at a) monthly, b) seasonal dry (JFMA), c) wet (JJAS) and d) annual timescales. Reconstructed coral SST at e, f) monthly, g, h) dry, i, j) wet, and k, l) annual shown temporally and compared to OISST. Seasonal dry, wet and annual RMSR of KOS_{RMSR} = 0.50 °C, 0.60 °C, 0.50 °C and WOL_{RMSR} = 0.60 °C, 0.60 °C, 0.50 °C shown in gray shadings, respectively. (For interpretation of the references to colour in this figure legend, the reader is referred to the web version of this article.)

the subsequent season, with different SST and Sr/Ca values and thus attenuation of the geochemical signals (Gagan et al., 2012). To estimate the duration of bio-smoothing within our sites, we divide the mean tissue layer thickness (6 mm year^{-1} for both corals) (i.e., (Lough and Barnes, 1997, 2000) over the mean linear extension rate. We found a greater influence of smoothing on WOL than on KOS, ~6.5 versus 4.5 months, respectively. The longer period in smoothing for WOL potentially results in a dampened seasonal Sr/Ca-SST slope.

Similar to past coral calibration studies (de Villiers et al., 1995; Linsley et al., 2006; Pfeiffer et al., 2009), our monthly regression equations for both KOS and WOL show independent coefficients, which may be caused by site-specific mean Sr/Ca offsets. KOS exhibits a greater mean Sr/Ca value (8.80 mmol/mol) than WOL (8.69 mmol/mol). We found that the mean values are consistent within a coral record even when averaged at shorter 10-year periods (1988–1998, 1998–2008), suggesting that the record length has minimal influence on mean Sr/Ca and that there is no measurable influence of diagenesis (Müller et al., 2001; Hendy et al., 2007; Sayani et al., 2011). Analytical precision is not the source of the Sr/Ca offset, which is seven times greater than our analytical error. Inter-laboratory comparisons between ASE and WHOI using both JCp-1 and Bunaken standards yield results within 1σ (see Methods), and therefore laboratory differences are not contributing to creating the offset. Both KOS and WOL are fast-growing corals and mean annual Sr/Ca does not correlate to linear extension rate (p = 0.55 and 0.44 for WOL and KOS, respectively). The insignificant relationship of Sr/Ca to linear extension suggests that observed offsets are not the result of growth-related effects, implying that other non-environmental effects may influence the offsets (Mitsuguchi et al., 2003; Allison and Finch, 2004). Nevertheless, the strong relationship between monthly Sr/Ca and instrumental SST, and calibration uncertainties less than 25% of the mean SST range (Table 1), indicates that monthly SST variability is reproducible.

3.2. Inter-annual Sr/Ca-SST calibrations

As monthly correlations are largely driven by the amplitude of the seasonal cycle (Crowley et al., 1999; Goodkin et al., 2005; Pfeiffer et al., 2009), we test the strength of the Sr/Ca-SST relationships by investigating interannual timescales. To derive Sr/Ca-SST calibrations based on interannual variability, 4-month wet season (JJAS), 4-month dry season (JFMA), and mean annual averages were determined based on precipitation climatologies (Fig. 1). Despite a ten-fold decrease in the number of observations from monthly to interannual timescales (dry season, wet season and mean annual), all of the Sr/Ca versus OISST interannual regressions indicate significant relationships (p < 0.05) (Fig. 4 b, c & d). The reconstructed interannual SSTs also display ENSO-influenced 4–6 year cycles, as observed in instrumental ENSO indices as well as coral-based interannual ENSO reconstructions (Cobb et al., 2003; Juillet-Leclerc et al., 2006; Quinn et al., 2006) (Fig. S3). The significant Sr/Ca-SST calibrations for KOS and WOL indicate that Sr/Ca is a robust paleothermometer, capturing interannual SST variability over multiple timescales (r = −0.64 to −0.70, p < 0.0001 WOL; r = −0.41 to −0.55, p < 0.05 KOS; Table 1).

To evaluate the interannual calibration equations further, we compared the differences between Sr/Ca-SST slopes at different timescales. The interannual Sr/Ca-SST slopes for KOS and WOL displayed different sensitivities but are within the expected range of past mean annual Sr/Ca-SST calibration studies (−0.05 to −0.10 mmol/mol/ 1 °C). Both KOS and WOL mean annual Sr/Ca-SST slopes increased in sensitivity to −0.080 mmol/mol °C^{-1} and -0.074 mmol/mol °C^{-1}, respectively. Dry season calibration slopes remained consistent with monthly calibration slopes, whereas the wet season slopes for both sites increased relative to monthly (Table 1). The wet season Sr/Ca-SST regression slopes may be steepened due to the narrow range of gridded SST (wet season OISST range = 1 °C) relative to local SST changes experienced at the study sites, which are in shallower water with a likely larger SST range.

Similarly, we examined the correlation and calibration errors across different timescales. Although all of the interannual calibration relationships are significant, the interannual WOL Sr/Ca-SST correlations mostly became stronger (monthly r = −0.65, p < 0.05; dry, wet and mean annual r = −0.70, −0.64, −0.70, p < 0.0005), whereas KOS Sr/Ca-SST correlations weakened (monthly r = −0.60, p < 0.05; dry, wet and mean annual r = −0.42, −0.55, −0.41, p < 0.05) (Table 1). The interannual calibration uncertainties (RMSR) of KOS increased by 10–49% relative to monthly timescales (Table 1). The weakened interannual Sr/Ca-SST relationship at KOS may be related to a number of potential causes: 1) the large gridded 1° × 1° OISST dataset may misrepresent local KOS SST changes; 2) the 'landmass effect' may influence local SST at KOS, where the coral is close to Kosrae Island, compared to Woleai Atoll which better represents open oceanographic conditions (Palacios, 2002; Elliott et al., 2012).

3.3. WPWP SST variability due to ENSO

To investigate changes in WPWP SST due to ENSO variability, we compared interannual SST reconstructions from WOL and KOS to the Niño 4 index. The Niño 4 index is calculated from SST anomalies over the central tropical Pacific within the 5°S-5°N, 160°E-150°W region (Trenberth and Stepaniak, 2001). El Niño (La Niña) events are defined by Niño4 SST anomalies above 0.4 °C (below −0.4 °C) over a 6-month period. To allow comparison of dry season coral reconstructed SST records during the Northern winter, a season when ENSO amplitude frequently peaks (Rasmusson and Carpenter, 1982; Trenberth, 1997), we averaged the JFMA months of Niño4 anomalies (Niño4$_{dry}$). Also, the coral SST records were normalized to calculate dry season anomalies by subtracting mean SST from each record and dividing by its standard deviation (WOL$_{dry}$, KOS$_{dry}$). KOS$_{dry}$ showed a positive correlation to Niño4$_{dry}$ (r = 0.54, p < 0.05, n = 25; Fig. 5a, e), while WOL$_{dry}$ in contrast, displayed a negative correlation to Niño4$_{dry}$ (r = −0.50, p < 0.05, n = 27; Fig. 5b, f). As predicted by the WPWP spatial SST composite maps (Fig. 2a, b), WOL records cool anomalies during El Niño events whereas KOS experiences warm anomalies. The reverse occurs during La Niña events at both sites.

To capture the spatial WPWP SST variability driven by ENSO, we subtracted the normalized SST anomalies of WOL$_{dry}$ from KOS$_{dry}$ to calculate a KOSWOL$_{SST}$ index. Correspondingly, we also derived KOSWOL$_{instrumental\ SST}$ index using gridded OISST from each site. The coral derived KOSWOL$_{SST}$ index shows a strong correlation to Niño4 (r = 0.63, p < 0.05, n = 25, Fig. 5c, g), greater than either site alone. The ability of the coral KOSWOL$_{SST}$ index to capture spatial WPWP SST variability is confirmed by its very strong correlation to KOSWOL$_{instrumental\ SST}$ (r = 0.77, p < 0.05, n = 25, Fig. 5d, h). These robust temporal and spatial SST relationships driven by ENSO (Fig. 5g, h) suggest an eastward expansion (contraction) of the WPWP during El Niño (La Niña) events.

3.4. Monthly seawater ($\delta^{18}O_{sw}$) reconstruction and calibration

Like Sr/Ca, the seasonal $\delta^{18}O_c$ ranges of 0.210‰ and 0.214‰ are similar for both sites, with values between −5.489 to −5.699‰ at KOS and − 5.458 to −5.672‰ at WOL.

Comparing the $\delta^{18}O_c$ records to the calculated instrumental pseudocoral time series validates the joint influence of SST and SSS on $\delta^{18}O_c$ for both KOS and WOL. (Supplementary Information). To remove the thermal effect from $\delta^{18}O_c$ and isolate the $\delta^{18}O_{sw}$ reflective of SSS, we followed the centering approach outlined by Cahyarini et al. (2008):

$$\delta^{18}O_{sw} = (\delta^{18}O_c - \overline{\delta^{18}O_c}) - \frac{\gamma}{\beta}(Sr/Ca - \overline{Sr/Ca}) \quad (5)$$

where $\delta^{18}O_{sw}$ is determined by removing the monthly Sr/Ca anomalies from $\delta^{18}O_c$ anomalies. γ is each site's $\delta^{18}O_c$–SST (Sr/Ca) slope (−0.082 and − 0.116‰ °C^{-1} for WOL and KOS, respectively) and β is the Sr/

Table 1
Pearson least square linear regression of Sr/Ca versus OISST and δ^{18}Osw versus SODA SSS for KOS and WOL at monthly, seasonal dry (JFMA), wet (JJAS) and annual timescales.

	Proxy = m * SST + b									
	m	1σ error (m)	b (y-intercept)	1σ error (b)	r	p	RMSR (°C)	Gridded SST range	Percentage error relative to SST range (%)	n
Monthly proxy data Sr/Ca (mmol/mol)										
KOS	−0.07	0.01	10.86	0.03	−0.60	< 0.01	0.6	2.5	24	300
WOL	−0.05	0.01	10.19	0.02	−0.65	< 0.01	0.6	2.8	21	324
Dry (JFMA)										
KOS	−0.05	0.02	10.24	0.10	−0.42	0.04	0.5	1.5	34	25
WOL	−0.07	0.01	10.61	0.07	−0.70	< 0.01	0.6	1.7	34	27
Wet (JJAS)										
KOS	−0.10	0.03	11.80	0.17	−0.55	0.004	0.6	1.0	56	25
WOL	−0.06	0.01	10.56	0.08	−0.64	< 0.01	0.6	1.0	62	27
Annual										
KOS	−0.08	0.04	11.14	0.19	0.41	0.04	0.5	0.6	73	25
WOL	−0.07	0.01	10.85	0.08	0.70	< 0.01	0.5	1.0	51	27
	Proxy = m * SSS + b									
	m	1σ error (m)	b (y-intercept)	1σ error (b)	r	p	RMSR (psu)	Gridded SSS range	Percentage error relative to SSS range (%)	n
Monthly proxy data $\delta^{18}O_{sw}$										
KOS	0.26	0.03	−8.95	0.15	0.50	< 0.01	0.3	1.6	17	300
WOL	0.30	0.03	−10.17	0.18	0.47	< 0.01	0.4	1.4	28	324
Dry (JFMA)										
KOS	0.29	0.12	−9.89	0.71	0.43	0.04	0.4	0.8	49	25
WOL	0.47	0.15	−16.15	0.15	0.53	< 0.01	0.3	0.5	53	27
Wet (JJAS)										
KOS	0.28	0.11	−9.52	0.62	0.46	0.02	0.4	0.9	45	25
WOL	0.23	0.07	−7.99	0.40	0.55	< 0.01	0.3	1.1	25	27
Annual										
KOS	0.36	0.11	−12.31	0.67	0.53	< 0.01	0.4	0.8	47	25
WOL	0.31	0.07	−10.58	0.42	0.64	< 0.01	0.2	0.8	23	27

Ca–SST slope (−0.052 and − 0.071 mmol/mol^{-1} °C for WOL and KOS, respectively). Type (II) Pearson's Major Axis linear regression of $\delta^{18}O_{sw}$ to SODA for WOL and KOS during the respective years (1986–2012 and 1988–2012) reveal significant relationships (Fig. 6a).

$$\text{WOL } \delta^{18}O_{sw} = 0.299\ (\pm 0.031) \times \text{SSS (psu)} - 10.168\ (\pm 0.180) \quad (6)$$

$r = 0.47$, $p < 0.0001$, RMSR = 0.40 psu, $n = 324$, SSS range = 1.4 psu, years = 1986-2012

$$\text{KOS } \delta^{18}O_{sw} = 0.261\ (\pm 0.026) \times \text{SSS (psu)} - 8.952\ (\pm 0.153) \quad (7)$$

$r = 0.50$, $p < 0.0001$, RMSR = 0.30 psu, $n = 300$, SSS range = 1.6 psu, years = 1988-2012

Recent in-situ studies across the tropical Pacific establish variable $\delta^{18}O_{sw}$-SSS slopes, which show an increasing trend from the eastern to western Pacific (Conroy et al., 2017). Both WOL and KOS monthly $\delta^{18}O_{sw}$-SSS slopes fall within previously reported slopes for the Western Pacific sites of Palau and Papua New Guinea (Morimoto et al., 2002; Conroy et al., 2014). While both corals have similar $\delta^{18}O_{sw}$ ranges, WOL located further west has a steeper slope (0.299‰ psu^{-1}) compared to KOS (0.261‰ psu^{-1}). The steeper slope for WOL is despite the higher salinity range, which results largely from higher observed precipitation changes compared to KOS (Fig. 1). To evaluate the robustness of the $\delta^{18}O_{sw}$-SSS calibration, interannual calibrations were investigated (dry season, wet season, and mean annual).

3.5. Reconstructing interannual $\delta^{18}O_{sw}$(SSS) at respective sites

Monthly $\delta^{18}O_{sw}$ was averaged for dry season (JFMA), wet season (JJAS), and mean annual timescales to create interannual time series. Despite a 90% decrease in observations, interannual $\delta^{18}O_{sw}$-SSS regressions remained significant ($p < 0.05$) (Fig. 6 b, c, and d). The interannual $\delta^{18}O_{sw}$-SSS relationships also remained consistent with minimal changes in correlation strength relative to monthly relationships (Table 1). Similar to SST reconstructions, all of the interannual (dry, wet and mean annual) SSS reconstructions showed 3–5 year interannual cycles (i.e., significant 3–5 year spectral frequencies) consistent with the influence of ENSO (Fig. S4) (Nurhati et al., 2011; Gorman et al., 2012). The significance and consistency of interannual $\delta^{18}O_{sw}$-SSS relationships imply a robust calibration, and the observed interannual SSS changes indicate that corals are capturing the influence of precipitation and (or) advection observed during ENSO years (Fig. 2c, d).

Past studies suggest that $\delta^{18}O_{sw}$-SSS slopes across the tropics vary with precipitation amount (Moerman et al., 2013; Conroy et al., 2017). To establish whether differences in interannual $\delta^{18}O_{sw}$-SSS sensitivities across the WPWP are driven by precipitation, we compared the slopes for interannual timescales to mean precipitation for each location and time. While we observed changes in slopes, a weak and insignificant correlation indicate that the differences in interannual slopes are not strongly influenced by differences in mean interannual precipitation

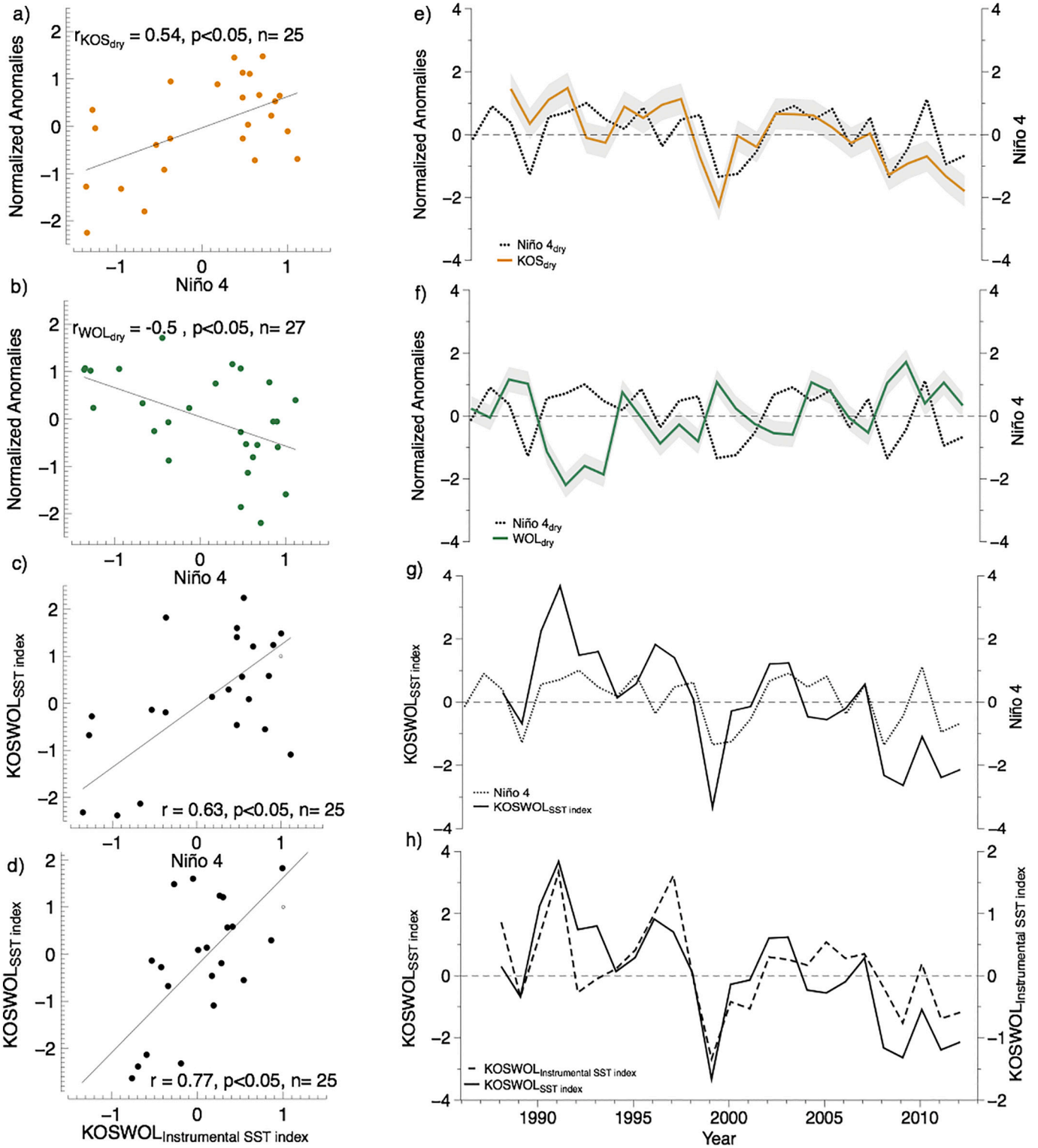

Fig. 5. Seasonal dry (JFMA) a) KOS (orange) and b) WOL (green) are significantly correlated with Niño 4 index. KOSWOL$_{SST}$ index is significantly correlated to c) Niño 4 and d) KOSWOL$_{instrumental\ SST\ index}$. Normalized SST anomalies of e) KOS (orange), f) WOL (green) and the Niño 4 (dotted) index versus time. Normalized SST anomalies of g) Niño 4 (dotted), h) KOSWOL$_{instrumental\ SST\ index}$ (dash) and KOSWOL$_{SST\ index}$ (black) versus time. Gray shading indicates standardized RMSR of KOS$_{dry}$ (0.5 °C) and WOL$_{dry}$ (0.6 °C), respectively. (For interpretation of the references to colour in this figure legend, the reader is referred to the web version of this article.)

($r = -0.40, p > 0.05, n = 8$) (Fig. S5). The changes in slopes may be related to the decreasing variance of the gridded SSS, which artificially steepens the $\delta^{18}O_{sw}$-SSS slopes. However, the insignificant correlation versus variance ($r = -0.67, p > 0.05$, n = 8) suggests that more observations are required to test both relationships.

3.6. WPWP SSS variability due to ENSO

To investigate the impact of ENSO on spatial and temporal variability in WPWP precipitation, KOS and WOL dry season SSS were compared to the El Niño Southern Oscillation Precipitation Index

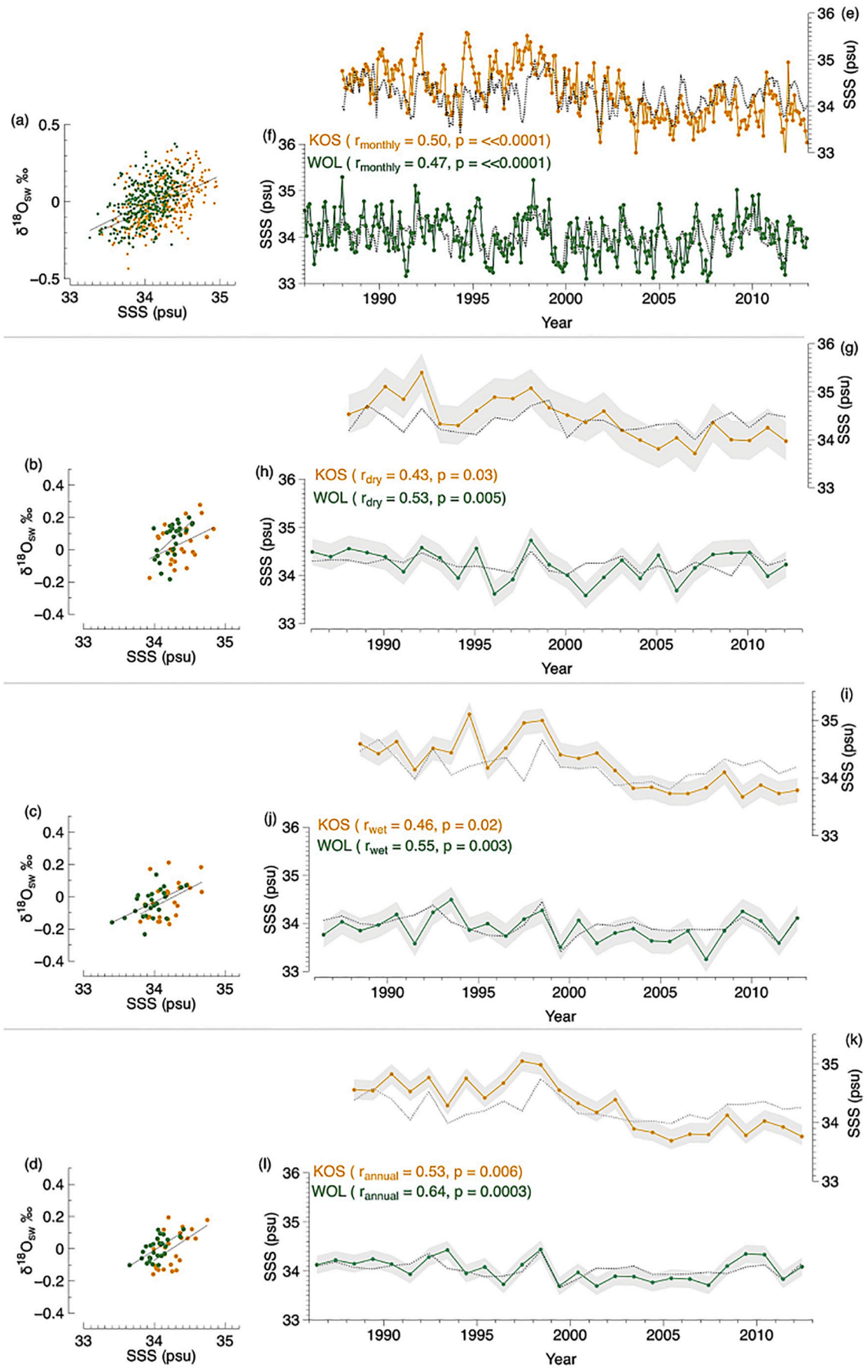

Fig. 6. $\delta^{18}O_{sw}$ (‰) from KOS (orange) and WOL (green) are significantly correlated to SODA SSS at a) monthly, b) seasonal dry (JFMA), c) wet (JJAS) and d) annual timescales. Reconstructed coral SSS (PSU) at e, f) monthly, g, h) dry, i, j) wet, and k, l) annual shown temporally and compared to SODA SSS. Seasonal dry, wet and annual RMSR for KOS_{RMSR} = 0.40 psu, 0.35 psu, 0.35 psu and WOL_{RMSR} = 0.30 psu, 0.30 psu, 0.20 psu shown in gray shadings, respectively.

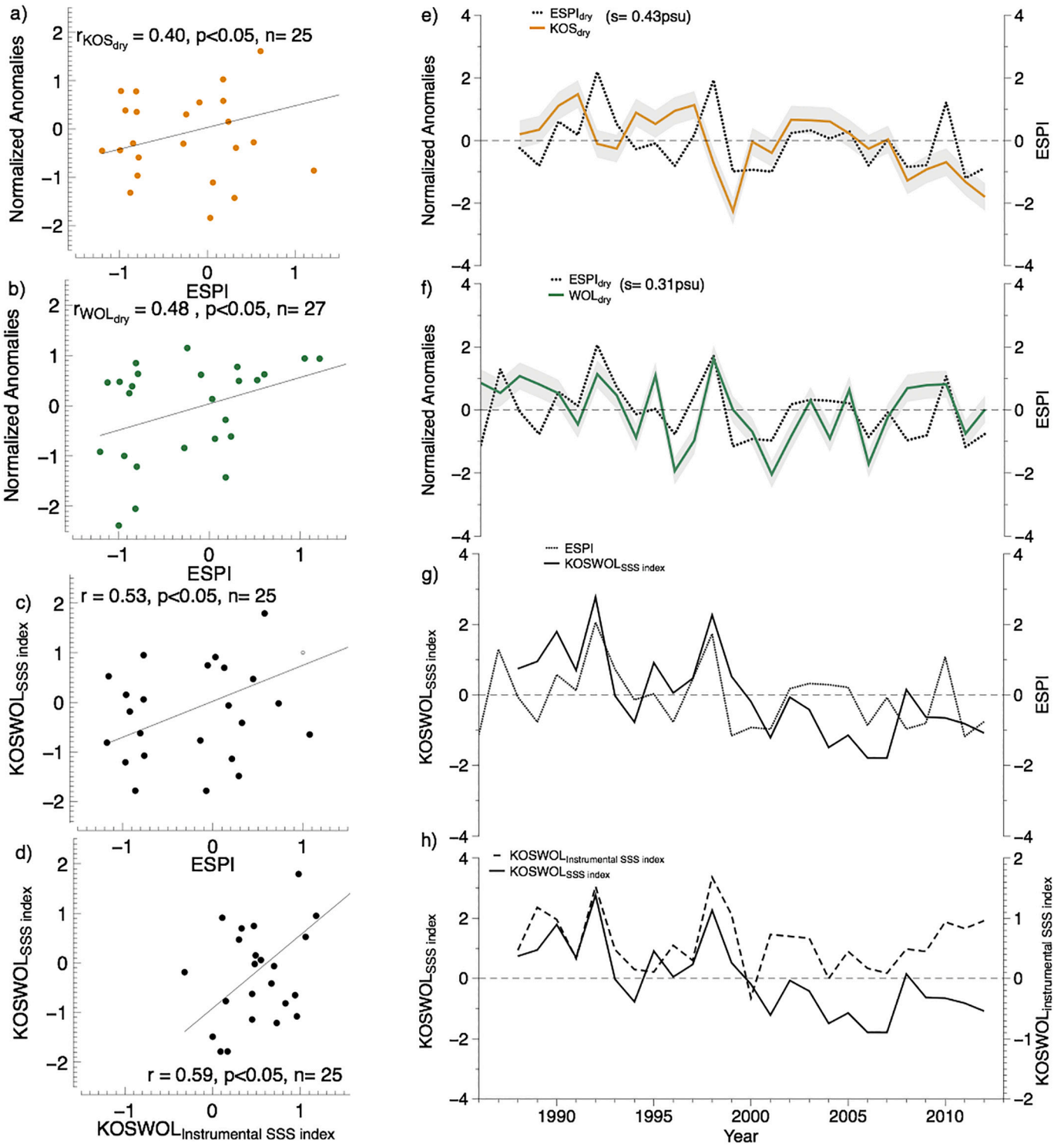

Fig. 7. Seasonal dry (JFMA) a) KOS (orange) and b) WOL (green) are significantly correlated with ESPI. $KOSWOL_{SSS}$ index is significantly correlated to c) ESPI and d) $KOSWOL_{instrumental\ SSS\ index}$. Normalized SSS anomalies of e) KOS (orange), f) WOL(green) and the ESPI (dotted) versus time. Normalized SSS anomalies of g) ESPI (dotted), h) $KOSWOL_{instrumental\ SSS\ index}$ (dash) and $KOSWOL_{SSS\ index}$ (black) versus time. Gray shading indicates standardized RMSR of KOS_{dry} (0.4‰) and WOL_{dry} (0.3‰), respectively. (For interpretation of the references to colour in this figure legend, the reader is referred to the web version of this article.)

(ESPI). ESPI tracks precipitation gradients between the Maritime Continent and the Equatorial Pacific region (Curtis and Adler, 2000). Positive (negative) ESPI values indicate El Niño (La Niña) phase of the ENSO cycle. Using an approach similar to comparing SST reconstructions and the Niño4 index during frequent ENSO peak amplitude, we normalized the dry season SSS reconstructions by removing the temporal mean and dividing the anomalies by the standard deviation (KOS_{dry} and WOL_{dry}). Similarly, we averaged the dry season months (JFMA) of ESPI to produce $ESPI_{dry}$. We observe positive correlations of both KOS_{dry} and WOL_{dry} to $ESPI_{dry}$ ($r = 0.40$, $p < 0.05$, $n = 25$, and $r = 0.48$, $p < 0.05$, $n = 27$, respectively) (Fig. 7a, b, e, f). These relationships indicate that dry season SSS records at KOS and WOL both capture anomalous precipitation changes driven by ENSO.

Similar to calculating the dry season $KOSWOL_{SST}$ gradient index, we

evaluated whether KOS and WOL together can capture additional WPWP regional SSS variability by averaging the normalized SSS anomalies of KOS_{dry} and WOL_{dry} to generate a $KOSWOL_{SSS}$ index (Fig. 7c). Comparably, we also derived $KOSWOL_{instrumental\ SSS}$ using gridded SODA SSS of each site. The $KOSWOL_{SSS}$ index shows a stronger correlation to ESPI ($r = 0.53$, $p < 0.05$, n = 25) than either coral site individually, demonstrating the value of multiple locations to capture spatial as well as temporal variability (Fig. 7c, g). The $KOSWOL_{SSS}$ index also showed comparable relationships to $KOSWOL_{instrumental\ SSS}$ ($r = 0.59$, $p < 0.05$, n = 25, Fig. 7d, h), reinforcing the importance of the coral index for capturing gridded SSS variability. Lastly, both $KOSWOL_{SSS}$ index and $KOSWOL_{instrumental\ SSS}$ showed significant relationships to Niño 1,2 ($r = 0.53$, $p < 0.05$, n = 25, and $r = 0.61$, $p < 0.05$, n = 25, respectively) (Fig. S6). These relationships imply ENSO driven Eastern Pacific SST anomalies may be phased locked to the WPWP hydrological changes.

4. Discussion

Our major findings are two-fold. First, coral proxies Sr/Ca and $\delta^{18}O_{sw}$ from both KOS and WOL sites are capable of accurately reconstructing climate variables SST and SSS at monthly and interannual (dry season, wet season, and mean annual) timescales, including the directions of change driven by ENSO events. Second, combining individual climate records from each site to generate spatial indices ($KOSWOL_{SST}$ and $KOSWOL_{SSS}$) captures the distinct spatial SST and SSS signatures within the WPWP caused by ENSO. For Sr/Ca, the multi-timescale calibrations to instrumental SST are all significant at both sites ($p < 0.05$). The difference between reconstructed dry season SST anomalies from both sites ($KOSWOL_{SST}$ index) is highly sensitive to the spatial migration of the WPWP influenced by ENSO and provides a valuable tool for reconstructing past ENSO behavior. Similarly, calibrations of $\delta^{18}O_{sw}$ to instrumental SSS at both sites are significant ($p < 0.05$) and have steep slopes reflective of high precipitation variability in the WPWP. The averaging of reconstructed dry season SSS anomalies from both sites ($KOSWOL_{SSS}$ index) also captures the spatial signature of SSS change in the WPWP, recording the pattern of precipitation extremes driven by ENSO, and providing another strong proxy for reconstructing spatial as well as temporal ENSO variability in the past. The strong relationships of coral-based spatial indices to gridded instrumental spatial indices further supports the corals' utility in tracking ENSO-driven changes. Future reconstructions of these spatial indices back through time will reveal detailed WPWP climate variability and changes in ENSO behavior in this important region over the past several centuries.

We observed no evidence of analytical or growth-related impacts influencing the mean Sr/Ca offset of 0.11 mmol/mol between KOS and WOL, despite similar ranges in SST. This difference is comparable to observed mean Sr/Ca offsets reported within colonies (DeLong et al., 2007), between colonies (Pfeiffer et al., 2009; Wu et al., 2014; Alpert et al., 2016; Sayani et al., 2019) and between sites (Linsley et al., 2006; Wu et al., 2013). Many studies suggest non-environmental 'vital effects' can influence the coral Sr/Ca-SST relationship and create offsets between nearby coral records (Gaetani and Cohen, 2006; Gagnon et al., 2007). We also observed weakened interannual Sr/Ca-SST correlations relative to monthly for KOS, which may be due to the greatly reduced range of SST variability, the influence of terrestrial area within a large 1° × 1° SST grid, or the impact of 'landmass' effects from Kosrae Island (Palacios, 2002; Elliott et al., 2012). Our multi-site study leaves room to speculate about spatiotemporal changes in seawater Sr/Ca ratios impacting mean Sr/Ca in corals (Shen et al., 1996; Sun et al., 2005). However, measurements of Sr/Ca in seawater within the WPWP are sparse, non-continuous, and distant from our study sites (de Villiers, 1999). Some studies recommend coral core replication to enhance climatic signals (Lough, 2004; DeLong et al., 2007; DeLong et al., 2011; Dassié et al., 2014), and we also recommend on-site monitoring of Sr/Ca in seawater to identify potential source variability related to coral Sr/Ca and prevent erroneous interpretations of paleorecords (Linsley et al., 2006; Quinn et al., 2006).

We also demonstrated that it is possible to remove the thermal component from $\delta^{18}O_c$ to derive regional hydrological records at these sites. Our corals' $\delta^{18}O_{sw}$–SSS sensitivities of 0.26 and 0.3‰ $^{\circ}C^{-1}$ for KOS and WOL, respectively, are consistent with steep slopes expected from the WPWP based on regional calibration studies (Le Bec et al., 2000; Kilbourne et al., 2004), in-situ seawater studies (Morimoto et al., 2002; Conroy et al., 2017) and simulated $\delta^{18}O_{sw}$–SSS in the WPWP (LeGrande and Schmidt, 2006). Depending on location, some calibration studies reported minimal or insignificant SST or SSS contributions to coral $\delta^{18}O$ and attributed $\delta^{18}O_c$ directly to a single variable (Le Bec et al., 2000; Wu and Grottoli, 2010; Dassié et al., 2014; Murty et al., 2017). Some studies removed the thermal component using instrumental SST (Iijima et al., 2005), while others found insignificant relationships between $\delta^{18}O_{sw}$ and gridded or in-situ SSS datasets (Quinn et al., 2006; Carilli et al., 2014). A lack of coral-derived $\delta^{18}O_{sw}$-SSS relationship in other locations has been explained by 1) overly coarse sampling from limited ship tracks to resolve local SSS changes (Quinn et al., 2006; Maes et al., 2013; Boutin et al., 2016); 2) thermal stress to the coral impacting the Sr/Ca-SST relationship used to remove SST from $\delta^{18}O_c$ (Marshall and McCulloch, 2002; Mitsuguchi et al., 2008; Sagar et al., 2016; Leupold et al., 2019); 3) low SST variability confounding the Sr/Ca signal for SST (Murty et al., 2018), compounded with analytical uncertainties ($\delta^{18}O_c$ & Sr/Ca) masking $\delta^{18}O_{sw}$ variability (Cahyarini et al., 2008); and 4) covariance between SST and SSS leading to changes in $\delta^{18}O$-SST (Osborne et al., 2014). Based on these potential influences, it is significant that coral $\delta^{18}O_{sw}$ showed significant relationships to gridded instrumental SSS and a regional precipitation index at both of our sites, despite being within a region of minimal SST variability. The strong $\delta^{18}O_{sw}$-SSS correlations seen here may be due to the high salinity variance within the region (Russon et al., 2013), resulting in a higher contribution of $\delta^{18}O_{sw}$, compared to SST, to the total $\delta^{18}O_c$. Multiple linear regression of $\delta^{18}O_c$ to instrumental SST and SSS provides evidence of a stronger SSS contribution than SST at both sites (Table S1). Nevertheless, the use of both SST and SSS in deriving the $\delta^{18}O_{pseudo}$ for age-modelling may have improved our $\delta^{18}O_c$ calibrations, as well as separation of SST and SSS variables to quantify the hydrological contribution. During data analysis, we evaluated several methods for age-modelling the coral proxies and realized that some methods (e.g., directly pairing only Sr/Ca to SST, $\delta^{18}O_c$ to SST, or $\delta^{18}O_c$ to SSS) biased the latter proxy-climate relationships. Thus, for sites with strong SSS variability, we recommend age-modelling proxy $\delta^{18}O_c$ to $\delta^{18}O_{pseudo}$ and then 'fine-tuning' Sr/Ca to SST to optimize reconstruction of both SST and SSS variables, as discussed in greater detail in the methods section.

Our multi-site coral indices track the zonal SST and SSS gradients within the WPWP, a key region regulating global climate teleconnections. The KOS and WOL sites, located near the heart of the warm pool itself, record hydrological changes due to zonal (east-west) migration of the WPWP during ENSO events. The strong correlations of the $KOSWOL_{SST}$ and $KOSWOL_{SSS}$ indices to the Niño 4 SST and ESPI SSS indices, respectively, show that we can derive past ENSO-driven spatial patterns with these corals. Consistent with Asami et al. (2004), our records show that not every reconstructed SST and SSS anomaly in the WPWP corresponds to a traditionally recognized ENSO event. Inferring from $KOSWOL_{SSS}$, the weak El Niño event in 1992 appears as a large positive anomaly in the WPWP, implying drier conditions in the WPWP comparable to the 'larger' 1997–1998 El Niño event. A positive anomaly in the instrumental $KOSWOL_{SSS}$ index (Fig. 7h) at the same time verifies the anomaly and signals the eastern expansion of the WPWP. This supports the interpretation that distinct ENSO variability occurring within the WPWP region may not be equally expressed in the central Pacific.

5. Conclusions

In this ~30-year coral calibration study, we investigated coral cores from two separate sites in the Federated States of Micronesia to evaluate whether an individual and multi-coral reconstructions capture regional climate behavior across the WPWP. Each coral is found to individually capture changes in SST (via Sr/Ca) and SSS (via conversion of $\delta^{18}O_c$ to $\delta^{18}O_{sw}$) at monthly to interannual timescales. Subsequently, these reconstructions of SSS and SST at each site reliably reconstruct ENSO as recorded in regional instrumental indices. More importantly, the difference between each site's dry season SST anomalies (KOSWO-L_{SST} index) tracks the spatial migration of the WPWP, and the average of SSS anomalies from both sites (KOSWOL$_{SSS}$ index) records the spatial SSS footprint, both due to ENSO variability. These climate gradients (KOSWOL$_{SST}$ index and KOSWOL$_{SSS}$ index) provide powerful tools for investigating past climate behavior in the WPWP, and ENSO expression in the western Pacific, over the past several centuries.

Declaration of Competing Interest

The authors declare that they have no known competing financial interests or personal relationships that could have appeared to influence the work reported in this paper.

Acknowledgements

We would like to thank two anonymous reviewers for their helpful comments that improved the manuscript. We also thank the crew of the *M/V Alucia* for assistance during the 2012 coral drilling expedition to FSM, funded by the Dalio Family Foundation through a WHOI Access to The Sea grant to KAH (#25110104). Geochemical analysis was funded by Singapore Ministry of Education Academic Research Fund Tier-2 (# MOE2016-T2-1016) to NFG and KAH, and by the WHOI Summer Student Fellowship Program (00450400) and Coastal Preservation Network 501c to IMS.

Appendix A. Supplementary data

Supplementary data to this article can be found online at https://doi.org/10.1016/j.palaeo.2020.110037.

References

Alibert, C., Kinsley, L., 2008. A 170-year Sr/Ca and Ba/Ca coral record from the western Pacific warm pool: 1. What can we learn from an unusual coral record? J. Geophys. Res. Oceans 113.
Alibert, C., McCulloch, M.T., 1997. Strontium/calcium ratios in modern Porites corals from the Great Barrier Reef as a proxy for sea surface temperature: calibration of the thermometer and monitoring of ENSO. Paleoceanography 12, 345–363.
Allison, N., Finch, A.A., 2004. High-resolution Sr/Ca records in modern Porites lobata corals: effects of skeletal extension rate and architecture. Geochem. Geophys. Geosyst. 5.
Alpert, A.E., Cohen, A.L., Oppo, D.W., DeCarlo, T.M., Gove, J.M., Young, C.W., 2016. Comparison of equatorial Pacific sea surface temperature variability and trends with Sr/Ca records from multiple corals. Paleoceanography 31, 252–265.
Anderson, W., Seager, R., Baethgen, W., Cane, M., You, L., 2019. Synchronous crop failures and climate-forced production variability. Sci. Adv. 5 (eaaw1976).
Anyamba, A., Chretien, J.-P., Britch, S.C., Soebiyanto, R.P., Small, J.L., Jepsen, R., Forshey, B.M., Sanchez, J.L., Smith, R.D., Harris, R., 2019. Global disease outbreaks associated with the 2015–2016 El Nino Event. Sci. Rep. 9, 1–14.
Asami, R., Yamada, T., Iryu, Y., Meyer, C.P., Quinn, T.M., Paulay, G., 2004. Carbon and oxygen isotopic composition of a Guam coral and their relationships to environmental variables in the western Pacific. Palaeogeogr. Palaeoclimatol. Palaeoecol. 212, 1–22.
Barr, C., Tibby, J., Leng, M., Tyler, J., Henderson, A., Overpeck, J., Simpson, G., Cole, J., Phipps, S., Marshall, J., 2019. Holocene el Niño–southern Oscillation variability reflected in subtropical Australian precipitation. Sci. Rep. 9, 1–9.
Beck, J.W., Edwards, R.L., Ito, E., Taylor, F.W., Recy, J., Rougerie, F., Joannot, P., Henin, C., 1992. Sea-surface temperature from coral skeletal strontium calcium ratios. Science 257, 644–647.
Bjerknes, J., 1966. A possible response of the atmospheric Hadley circulation to equatorial anomalies of ocean temperature. Tellus 18, 820–829.
Bjerknes, J., 1969. Atmospheric teleconnections from the equatorial Pacific. Mon. Weather Rev. 97, 163–172.
Bolton, A., Goodkin, N., Hughen, K., Ostermann, D., Vo, S., Phan, H., 2014. Paired Porites coral Sr/Ca and δ 18 O from the western South China Sea: Proxy calibration of sea surface temperature and precipitation. Palaeogeogr. Palaeoclimatol. Palaeoecol. 410, 233–243.
Boutin, J., Chao, Y., Asher, W., Delcroix, T., Drucker, R., Drushka, K., Kolodziejczyk, N., Lee, T., Reul, N., Reverdin, G., 2016. Satellite and in situ salinity: understanding near-surface stratification and subfootprint variability. Bull. Am. Meteorol. Soc. 97, 1391–1407.
Brakenridge, G., Syvitski, J., Niebuhr, E., Overeem, I., Higgins, S., Kettner, A., Prades, L., 2017. Design with nature: causation and avoidance of catastrophic flooding, Myanmar. Earth Sci. Rev. 165, 81–109.
Brenner, L.D., Linsley, B.K., Potts, D.C., 2017. A modern Sr/Ca-δ18O-sea surface temperature calibration for Isopora corals on the Great Barrier Reef. Paleoceanography 32, 182–194.
Brook, G.A., Rafter, M.A., Railsback, L.B., Sheen, S.-W., Lundberg, J., 1999. A high-resolution proxy record of rainfall and ENSO since AD 1550 from layering in stalagmites from Anjohibe Cave, Madagascar. The Holocene 9, 695–705.
Cahyarini, S.Y., Pfeiffer, M., Timm, O., Dullo, W.-C., Schönberg, D.G., 2008. Reconstructing seawater δ18O from paired coral δ18O and Sr/Ca ratios: Methods, error analysis and problems, with examples from Tahiti (French Polynesia) and Timor (Indonesia). Geochim. Cosmochim. Acta 72, 2841–2853.
Cahyarini, S.Y., Pfeiffer, M., Dullo, W.-C., 2009. Improving SST reconstructions from coral Sr/ca records: multiple corals from Tahiti (French Polynesia). Int. J. Earth Sci. 98, 31–40.
Cane, M.A., 1986. El Niño. Annu. Rev. Earth Planet. Sci. 14, 43–70.
Capotondi, A., Wittenberg, A.T., Newman, M., Di Lorenzo, E., Yu, J.-Y., Braconnot, P., Cole, J., Dewitte, B., Giese, B., Guilyardi, E., 2015. Understanding ENSO diversity. Bull. Am. Meteorol. Soc. 96, 921–938.
Carilli, J.E., McGregor, H.V., Gaudry, J.J., Donner, S.D., Gagan, M.K., Stevenson, S., Wong, H., Fink, D., 2014. Equatorial Pacific coral geochemical records show recent weakening of the Walker Circulation. Paleoceanography 29, 1031–1045.
Carricart-Ganivet, J.P., Barnes, D.J., 2007. Densitometry from digitized images of X-radiographs: Methodology for measurement of coral skeletal density. J. Exp. Mar. Biol. Ecol. 344, 67–72.
Carton, J., Chepurin, G., Chen, L., 2016. An Updated Reanalysis of Ocean Climate using the Simple Ocean Data Assimilation version 3 (SODA3). (manuscript in preparation).
Chen, S., Hoffmann, S.S., Lund, D.C., Cobb, K.M., Emile-Geay, J., Adkins, J.F., 2016. A high-resolution speleothem record of western equatorial Pacific rainfall: implications for Holocene ENSO evolution. Earth Planet. Sci. Lett. 442, 61–71.
Cobb, K.M., Charles, C.D., Cheng, H., Edwards, R.L., 2003. El Nino/Southern Oscillation and tropical Pacific climate during the last millennium. Nature 424, 271–276.
Cobb, K.M., Westphal, N., Sayani, H.R., Watson, J.T., Di Lorenzo, E., Cheng, H., Edwards, R., Charles, C.D., 2013. Highly variable El Niño–southern oscillation throughout the Holocene. Science 339, 67–70.
Cohen, A.L., Layne, G.D., Hart, S.R., Lobel, P.S., 2001. Kinetic control of skeletal Sr/Ca in a symbiotic coral: implications for the paleotemperature proxy. Paleoceanography 16, 20–26.
Cohen, A.L., Owens, K.E., Layne, G.D., Shimizu, N., 2002. The effect of algal symbionts on the accuracy of Sr/Ca paleotemperatures from coral. Science 296, 331–333.
Cole, J.E., Fairbanks, R.G., Shen, G.T., 1993. Recent variability in the Southern Oscillation: isotopic results from a Tarawa Atoll coral. Science 260, 1790–1794.
Conroy, J.L., Overpeck, J.T., Cole, J.E., Shanahan, T.M., Steinitz-Kannan, M., 2008. Holocene changes in eastern tropical Pacific climate inferred from a Galápagos lake sediment record. Quat. Sci. Rev. 27, 1166–1180.
Conroy, J.L., Cobb, K.M., Lynch-Stieglitz, J., Polissar, P.J., 2014. Constraints on the salinity–oxygen isotope relationship in the central tropical Pacific Ocean. Mar. Chem. 161, 26–33.
Conroy, J.L., Thompson, D.M., Cobb, K.M., Noone, D., Rea, S., Legrande, A.N., 2017. Spatiotemporal variability in the δ18O-salinity relationship of seawater across the tropical Pacific Ocean. Paleoceanography 32, 484–497.
Cook, E.R., Krusic, P.J., Jones, P.D., 2003. Dendroclimatic signals in long tree-ring chronologies from the Himalayas of Nepal. Int. J. Climatol. 23, 707–732.
Cook, E.R., Buckley, B.M., Palmer, J.G., Fenwick, P., Peterson, M.J., Boswijk, G., Fowler, A., 2006. Millennia-long tree-ring records from Tasmania and New Zealand: a basis for modelling climate variability and forcing, past, present and future. J. Quater. Sci. Publ. Quater. Res. Assoc. 21, 689–699.
Corrège, T., Delcroix, T., Recy, J., Beck, W., Cabioch, G., Le Cornec, F., 2000. Evidence for stronger El Nino-Southern Oscillation (ENSO) events in a mid-Holocene massive coral. Paleoceanography 15, 465–470.
Corrège, T., Gagan, M.K., Beck, J.W., Burr, G.S., Cabioch, G., Le Cornec, F., 2004. Interdecadal variation in the extent of South Pacific tropical waters during the Younger Dryas event. Nature 428, 927–929.
Cravatte, S., Delcroix, T., Dongxiao, Z., McPhaden, M., Leloup, J., 2009. Observed freshening and warming of the western Pacific Warm Pool. Clim. Dyn. 33, 565–589.
Crowley, T.J., Quinn, T.M., Hyde, W.T., 1999. Validation of coral temperature calibrations. Paleoceanography 14, 605–615.
Curtis, S., Adler, R., 2000. ENSO indices based on patterns of satellite-derived precipitation. J. Clim. 13, 2786–2793.
D'Arrigo, R., Cook, E.R., Wilson, R.J., Allan, R., Mann, M.E., 2005. On the variability of ENSO over the past six centuries. Geophys. Res. Lett. 32.
D'Arrigo, R., Wilson, R., Palmer, J., Krusic, P., Curtis, A., Sakulich, J., Bijaksana, S., Zulaikah, S., Ngkoimani, L.O., 2006. Monsoon drought over Java, Indonesia, during the past two centuries. Geophys. Res. Lett. 33.
Dassié, E.P., Linsley, B.K., Corrège, T., Wu, H.C., Lemley, G.M., Howe, S., Cabioch, G.,

2014. A Fiji multi-coral δ18O composite approach to obtaining a more accurate reconstruction of the last two-centuries of the ocean-climate variability in the South Pacific Convergence Zone region. Paleoceanography 29, 1196–1213.
de Villiers, S., 1999. Seawater strontium and Sr/Ca variability in the Atlantic and Pacific oceans. Earth Planet. Sci. Lett. 171, 623–634.
de Villiers, S., Nelson, B.K., Chivas, A.R., 1995. Biological controls on coral Sr/Ca and δ18O reconstructions of sea surface temperatures. Science 269, 1247–1249.
Delcroix, T., 1998. Observed surface oceanic and atmospheric variability in the tropical Pacific at seasonal and ENSO timescales: a tentative overview. J. Geophys. Res. Oceans 103, 18611–18633.
Delcroix, T., Henin, C., 1991. Seasonal and interannual variations of sea surface salinity in the tropical Pacific Ocean. J. Geophys. Res. Oceans 96, 22135–22150.
Delcroix, T., McPhaden, M., 2002. Interannual sea surface salinity and temperature changes in the western Pacific warm pool during 1992–2000. J. Geophys. Res. Oceans 107 (SRF 3-1-SRF 3–17).
DeLong, K., Quinn, T.M., Taylor, F.W., 2007. Reconstructing twentieth-century sea surface temperature variability in the Southwest Pacific: a replication study using multiple coral Sr/Ca records from New Caledonia. Paleoceanography 22.
DeLong, K., Flannery, J.A., Maupin, C.R., Poore, R.Z., Quinn, T.M., 2011. A coral Sr/Ca calibration and replication study of two massive corals from the Gulf of Mexico. Palaeogeogr. Palaeoclimatol. Palaeoecol. 307, 117–128.
DeLong, K., Quinn, T.M., Taylor, F.W., Lin, K., Shen, C.-C., 2012. Sea surface temperature variability in the southwest tropical Pacific since AD 1649. Nat. Clim. Chang. 2, 799–804.
DeLong, K., Quinn, T.M., Taylor, F.W., Shen, C.-C., Lin, K., 2013. Improving coral-base paleoclimate reconstructions by replicating 350 years of coral Sr/Ca variations. Palaeogeogr. Palaeoclimatol. Palaeoecol. 373, 6–24.
Dunbar, R.B., Wellington, G.M., Colgan, M.W., Glynn, P.W., 1994. Eastern Pacific Sea surface temperature since 1600 AD: the δ18O record of climate variability in Galápagos corals. Paleoceanography 9, 291–315.
Eldin, G., Delcroix, T., Rodier, M., 2004. The frontal area at the eastern edge of the western equatorial Pacific warm pool in April 2001. J. Geophys. Res. Oceans 109.
Elliott, J., Patterson, M., Gleiber, M., 2012. Detecting island mass effect through remote sensing. In: Proceedings of the 12th International Coral Reef Symposium.
Emile-Geay, J., Cobb, K.M., Mann, M.E., Wittenberg, A.T., 2013. Estimating central equatorial Pacific SST variability over the past millennium. Part II: reconstructions and implications. J. Clim. 26, 2329–2352.
Enfield, D.B., Lee, S.-K., Wang, C., 2006. How are large western hemisphere warm pools formed? Prog. Oceanogr. 70, 346–365.
Epstein, S., Buchsbaum, R., Lowenstam, H.A., Urey, H.C., 1953. Revised carbonate-water isotopic temperature scale. Geol. Soc. Am. Bull. 64, 1315–1326.
Fallon, S.J., McCulloch, M.T., Alibert, C., 2003. Examining water temperature proxies in Porites corals from the Great Barrier Reef: a cross-shelf comparison. Coral Reefs 22, 389–404.
Felis, T., Lohmann, G., Kuhnert, H., Lorenz, S.J., Scholz, D., Pätzold, J., Al-Rousen, S.A., Al-Moghrabl, S.M., 2004. Increased seasonality in Middle East temperatures during the last interglacial period. Nature 429, 164–168.
Gaetani, G.A., Cohen, A.L., 2006. Element partitioning during precipitation of aragonite from seawater: a framework for understanding paleoproxies. Geochim. Cosmochim. Acta 70, 4617–4634.
Gagan, M.K., Ayliffe, L.K., Hopley, D., Cali, J.A., Mortimer, G.E., Chappell, J., McCulloch, M.T., Head, M.J., 1998. Temperature and surface-ocean water balance of the mid-Holocene tropical western Pacific. Science 279, 1014–1018.
Gagan, M.K., Dunbar, G.B., Suzuki, A., 2012. The effect of skeletal mass accumulation in Porites on coral Sr/Ca and δ18O paleothermometry. Paleoceanography 27.
Gagnon, A.C., Adkins, J.F., Fernandez, D.P., Robinson, L.F., 2007. Sr/Ca and Mg/Ca vital effects correlated with skeletal architecture in a scleractinian deep-sea coral and the role of Rayleigh fractionation. Earth Planet. Sci. Lett. 261, 280–295.
Giuliani, M., Zaniolo, M., Castelletti, A., Davoli, G., Block, P., 2019. Detecting the state of the climate system via artificial intelligence to improve seasonal forecasts and inform reservoir operations. Water Resour. Res. 11, 9133–9147.
Goodkin, N.F., Hughen, K.A., Cohen, A.L., Smith, S.R., 2005. Record of Little Ice Age Sea surface temperatures at Bermuda using a growth-dependent calibration of coral Sr/Ca. Paleoceanography 20.
Goodkin, N.F., Hughen, K.A., Cohen, A.L., 2007. A multicoral calibration method to approximate a universal equation relating Sr/Ca and growth rate to sea surface temperature. Paleoceanography 22.
Gorman, M.K., Quinn, T.M., Taylor, F.W., Partin, J.W., Cabioch, G., Austin, J.A., Pelletier, B., Ballu, V., Maes, C., Saustrup, S., 2012. A coral-based reconstruction of sea surface salinity at Sabine Bank, Vanuatu from 1842 to 2007 CE. Paleoceanography 27 (n/a-n/a).
Grothe, P.R., Cobb, K.M., Liguori, G., Di Lorenzo, E., Capotondi, A., Lu, Y., Cheng, H., Edwards, R.L., Southon, J.R., Santos, G.M., 2020. Enhanced El Niño–Southern oscillation variability in recent decades. Geophys. Res. Lett. 47 (7) p.e2019GL083906.
Grove, C.A., Kasper, S., Zinke, J., Pfeiffer, M., Garbe-Schönberg, D., Brummer, G.J.A., 2013. Confounding effects of coral growth and high SST variability on skeletal Sr/Ca: implications for coral paleothermometry. Geochem. Geophys. Geosyst. 14, 1277–1293.
Hathorne, E.C., Gagnon, A., Felis, T., Adkins, J., Asami, R., Boer, W., Caillon, N., Case, D., Cobb, K.M., Douville, E., 2013. Interlaboratory study for coral Sr/Ca and other element/Ca ratio measurements. Geochem. Geophys. Geosyst. 14, 3730–3750.
Heiss, G., Camoin, G., Eisenhauer, A., Wischow, D., Dullo, C., Hansen, B., 1997. Stable Isotope and Sr/Ca-Signals in Corals from the Indian Ocean. Smithsonian Tropical Research Institute.
Hendy, E.J., Gagan, M.K., Alibert, C.A., McCulloch, M.T., Lough, J.M., Isdale, P.J., 2002. Abrupt decrease in tropical Pacific Sea surface salinity at end of Little Ice Age. Science 295, 1511–1514.
Hendy, E., Gagan, M., Lough, J., McCulloch, M., DeMenocal, P., 2007. Impact of skeletal dissolution and secondary aragonite on trace element and isotopic climate proxies in Porites corals. Paleoceanography 22.
Hennekam, R., Zinke, J., van Sebille, E., ten Have, M., Brummer, G.J.A., Reichart, G.J., 2018. Cocos (Keeling) corals reveal 200 years of multidecadal modulation of Southeast Indian Ocean hydrology by Indonesian throughflow. Paleoceanogr. Paleoclimatol. 33, 48–60.
Hu, Wu, L., Cai, W., Gupta, A.S., Ganachaud, A., Qiu, B., Gordon, A.L., Lin, X., Chen, Z., Hu, S., 2015. Pacific western boundary currents and their roles in climate. Nature 522, 299–308.
Hu, Hu, D., Guan, C., Xing, N., Li, J., Feng, J., 2017. Variability of the western Pacific warm pool structure associated with El Niño. Clim. Dyn. 49, 2431–2449.
Hughen, K.A., Schrag, D.P., Jacobsen, S.B., Hantoro, W., 1999. El Nino during the last interglacial period recorded by a fossil coral from Indonesia. Geophys. Res. Lett. 26, 3129–3132.
Iijima, H., Kayanne, H., Morimoto, M., Abe, O., 2005. Interannual sea surface salinity changes in the western Pacific from 1954 to 2000 based on coral isotope analysis. Geophys. Res. Lett. 32.
Janowiak E, John, Xie, Pingping, 1999. CAMS–OPI: A global satellite–rain gauge merged product for real-time precipitation monitoring applications. Journal of Climate 12 (11), 3335–3342 In press.
Juillet-Leclerc, A., Thiria, S., Naveau, P., Delcroix, T., Le Bec, N., Blamart, D., Correge, T., 2006. SPCZ migration and ENSO events during the 20th century as revealed by climate proxies from a Fiji coral. Geophys. Res. Lett. 33.
Kao, H.Y., Lagerloef, G.S., 2015. Salinity fronts in the tropical P acific O cean. J. Geophys. Res. Oceans 120, 1096–1106.
Kidwell, A., Han, L., Jo, Y.-H., Yan, X.-H., 2017. Decadal western Pacific warm pool variability: a centroid and heat content study. Sci. Rep. 7, 1–9.
Kilbourne, K.H., Quinn, T.M., Taylor, F.W., Delcroix, T., Gouriou, Y., 2004. El Nino–Southern Oscillation–related salinity variations recorded in the skeletal geochemistry of a Porites coral from Espiritu Santo, Vanuatu. Paleoceanography 19.
Knutson, D.W., Buddemeier, R.W., Smith, S.V., 1972. Coral chronometers: seasonal growth bands in reef corals. Science 177, 270–272.
Koutavas, A., Joanides, S., 2012. El Niño–Southern oscillation Extrema in the holocene and last glacial maximum. Paleoceanography 27.
Kuffner, I.B., Roberts, K.E., Flannery, J.A., Morrison, J.M., Richey, J.N., 2017. Fidelity of the S r/C a proxy in recording ocean temperature in the western a tlantic coral S iderastrea siderea. Geochem. Geophys. Geosyst. 18, 178–188.
Lachniet, M.S., Burns, S.J., Piperno, D.R., Asmerom, Y., Polyak, V.J., Moy, C.M., Christenson, K., 2004. A 1500-year El Niño/Southern Oscillation and rainfall history for the isthmus of Panama from speleothem calcite. J. Geophys. Res.-Atmos. 109.
Lam, H.C.Y., Haines, A., McGregor, G., Chan, E.Y.Y., Hajat, S., 2019. Time-series study of associations between rates of people affected by disasters and the El Niño Southern Oscillation (ENSO) cycle. Int. J. Environ. Res. Public Health 16, 3146.
Le Bec, N., Julliet-Leclerc, A., Corrège, T., Blamart, D., Delcroix, T., 2000. A coral δ18O record of ENSO driven sea surface salinity variability in Fiji (south-western tropical Pacific). Geophys. Res. Lett. 27, 3897–3900.
Leclerc, Schmidt, G., 2001. A calibration of the oxygen isotope paleothermometer of coral aragonite from Porites. Geophys. Res. Lett. 28, 4135–4138.
LeGrande, A.N., Schmidt, G.A., 2006. Global gridded data set of the oxygen isotopic composition in seawater. Geophys. Res. Lett. 33.
Leupold, M., Pfeiffer, M., Garbe-Schönberg, D., Sheppard, C., 2019. Reef-Scale-Dependent response of massive porites corals from the Central Indian Ocean to prolonged thermal stress: evidence from Coral Sr/Ca measurements. Geochem. Geophys. Geosyst. 20, 1468–1484.
Li, J., Xie, S.-P., Cook, E.R., Huang, G., D'arrigo, R., Liu, F., Ma, J., Zheng, X.-T., 2011. Interdecadal modulation of El Niño amplitude during the past millennium. Nat. Clim. Chang. 1, 114–118.
Linsley, B.K., Ren, L., Dunbar, R.B., Howe, S.S., 2000. El Niño Southern Oscillation (ENSO) and decadal-scale climate variability at 10° N in the eastern Pacific from 1893 to 1994: a coral-based reconstruction from Clipperton Atoll. Paleoceanography 15, 322–335.
Linsley, B.K., Wellington, G., Schrag, D., Ren, L., Salinger, M., Tudhope, A., 2004. Geochemical evidence from corals for changes in the amplitude and spatial pattern of South Pacific interdecadal climate variability over the last 300 years. Clim. Dyn. 22, 1–11.
Linsley, B.K., Kaplan, A., Gouriou, Y., Salinger, J., Demenocal, P.B., Wellington, G.M., Howe, S.S., 2006. Tracking the extent of the South Pacific Convergence Zone since the early 1600s. Geochem. Geophys. Geosyst. 7.
Liu, Kojima, K., Yoshimura, K., Oka, A., 2014. Proxy interpretation of coral-recorded seawater δ18O using 1-D model forced by isotope-incorporated GCM in tropical oceanic regions. J. Geophys. Res.-Atmos. 119, 12,021–012,033.
Lough, J.M., 2004. A strategy to improve the contribution of coral data to high-resolution paleoclimatology. Palaeogeogr. Palaeoclimatol. Palaeoecol. 204, 115–143.
Lough, J.M., Barnes, D., 1997. Several centuries of variation in skeletal extension, density and calcification in massive Porites colonies from the Great Barrier Reef: a proxy for seawater temperature and a background of variability against which to identify unnatural change. J. Exp. Mar. Biol. Ecol. 211, 29–67.
Lough, J.M., Barnes, D., 2000. Environmental controls on growth of the massive coral Porites. J. Exp. Mar. Biol. Ecol. 245, 225–243.
Lu, Z., Liu, Z., Zhu, J., Cobb, K.M., 2018. A review of paleo El Niño-Southern Oscillation. Atmosphere 9, 130.
Maes, C., Picaut, J., Kuroda, Y., Ando, K., 2004. Characteristics of the convergence zone at the eastern edge of the Pacific warm pool. Geophys. Res. Lett. 31.
Maes, C., Dewitte, B., Sudre, J., Garçon, V., Varillon, D., 2013. Small-scale features of

temperature and salinity surface fields in the Coral Sea. J. Geophys. Res. Oceans 118, 5426–5438.
Marshall, J.F., McCulloch, M.T., 2001. Evidence of El Nino and the Indian Ocean Dipole from Sr/Ca derived SSTs for modern corals at Christmas Island, eastern Indian Ocean. Geophys. Res. Lett. 28, 3453–3456.
Marshall, J.F., McCulloch, M.T., 2002. An assessment of the Sr/Ca ratio in shallow water hermatypic corals as a proxy for sea surface temperature. Geochim. Cosmochim. Acta 66, 3263–3280.
McCulloch, M.T., Gagan, M.K., Mortimer, G.E., Chivas, A.R., Isdale, P.J., 1994. A High-Resolution Sr/Ca and Delta-O-18 Coral Record from the Great-Barrier-Reef, Australia, and the 1982-1983 El-Nino. Geochim. Cosmochim. Acta 58, 2747–2754.
McGregor, H.V., Gagan, M.K., 2004. Western Pacific coral δ18O records of anomalous Holocene variability in the El Niño–Southern Oscillation. Geophys. Res. Lett. 31.
McGregor, S., Timmermann, A., Timm, O., 2009. A unified proxy for ENSO and PDO variability since 1650. Clim. Past Discuss. 5.
McGregor, H., Fischer, M.J., Gagan, M., Fink, D., Phipps, S.J., Wong, H., Woodroffe, C., 2013. A weak El Niño/Southern Oscillation with delayed seasonal growth around 4,300 years ago. Nat. Geosci. 6, 949.
McKibben, S.M., Peterson, W., Wood, A.M., Trainer, V.L., Hunter, M., White, A.E., 2017. Climatic regulation of the neurotoxin domoic acid. Proc. Natl. Acad. Sci. 114, 239–244.
McPhaden, M.J., 1999. Genesis and evolution of the 1997-98 El Niño. Science 283, 950–954.
McPhaden, M.J., 2018. Understanding and predicting El Niño and the Southern Oscillation. New Front. Oper. Oceanogr. 653–662.
McPhaden, M.J., Picaut, J., 1990. El Niño-Southern Oscillation displacements of the western equatorial Pacific warm pool. Science 250, 1385–1388.
McPhaden, M.J., Zebiak, S.E., Glantz, M.H., 2006. ENSO as an integrating concept in earth science. Science 314, 1740–1745.
Mitsuguchi, T., Matsumoto, E., Uchida, T., 2003. Mg/Ca and Sr/Ca ratios of Porites coral skeleton: Evaluation of the effect of skeletal growth rate. Coral Reefs 22, 381–388.
Mitsuguchi, T., Dang, P.X., Kitagawa, H., Uchida, T., Shibata, Y., 2008. Coral Sr/Ca and Mg/Ca records in Con Dao Island off the Mekong Delta: assessment of their potential for monitoring ENSO and East Asian monsoon. Glob. Planet. Chang. 63, 341–352.
Moerman, J.W., Cobb, K.M., Adkins, J.F., Sodemann, H., Clark, B., Tuen, A.A., 2013. Diurnal to interannual rainfall δ18O variations in northern Borneo driven by regional hydrology. Earth Planet. Sci. Lett. 369, 108–119.
Morimoto, M., Abe, O., Kayanne, H., Kurita, N., Matsumoto, E., Yoshida, N., 2002. Salinity records for the 1997–98 El Niño from Western Pacific corals. Geophys. Res. Lett. 29 (35–31–35-34).
Moy, C.M., Seltzer, G.O., Rodbell, D.T., Anderson, D.M., 2002. Variability of El Niño/Southern Oscillation activity at millennial timescales during the Holocene epoch. Nature 420, 162–165.
Müller, A., Gagan, M.K., McCulloch, M.T., 2001. Early marine diagenesis in corals and geochemical consequences for paleoceanographic reconstructions. Geophys. Res. Lett. 28, 4471–4474.
Murty, S.A., Goodkin, N.F., Halide, H., Natawidjaja, D., Suwargadi, B., Suprihanto, I., Prayudi, D., Switzer, A.D., Gordon, A., 2017. Climatic influences on southern Makassar Strait salinity over the past century. Geophys. Res. Lett. 44.
Murty, S.A., Goodkin, N.F., Wiguna, A., Gordon, A.L., 2018. Variability in Coral-Reconstructed Sea Surface Salinity between the Northern and Southern Lombok Strait Linked to East Asian Winter Monsoon mean State Reversals. Paleoceanogr. Paleoclimatol. 33, 1116–1133.
Newman, M., Wittenberg, A.T., Cheng, L., Compo, G.P., Smith, C.A., 2018. The extreme 2015/16 El Niño, in the context of historical climate variability and change. Bull. Am. Meteorol. Soc. 99, S16–S20.
Nurhati, I.S., Cobb, K.M., Di Lorenzo, E., 2011. Decadal-scale SST and salinity variations in the central tropical Pacific: Signatures of natural and anthropogenic climate change. J. Clim. 24, 3294–3308.
Okai, T., Suzuki, A., Kawahata, H., Terashima, S., Imai, N., 2002. Preparation of a new geological survey of Japan geochemical reference material: coral JCp-1. Geostand. Newslett. 26, 95–99.
Osborne, M.C., Dunbar, R.B., Mucciarone, D.A., Druffel, E., Sanchez-Cabeza, J.-A., 2014. A 215-yr coral δ18O time series from Palau records dynamics of the West Pacific Warm Pool following the end of the Little Ice Age. Coral Reefs 33, 719–731.
Paillard, D., Labeyrie, L., Yiou, P., 1996. Macintosh program performs time-series analysis. EOS Trans. Am. Geophys. Union 77 (39), 379.
Palacios, D.M., 2002. Factors influencing the island-mass effect of the Galápagos Archipelago. Geophys. Res. Lett. 29.
Partin, J.W., Quinn, T.M., Shen, C., Emile-Geay, J., Taylor, F.W., Maupin, C., Lin, K., Jackson, C.S., Banner, J.L., Sinclair, D., 2013. Multidecadal rainfall variability in South Pacific Convergence Zone as revealed by stalagmite geochemistry. Geology 41, 1143–1146.
Pfeiffer, M., Dullo, W.-C., Zinke, J., Garbe-Schönberg, D., 2009. Three monthly coral Sr/Ca records from the Chagos Archipelago covering the period of 1950–1995 a.D.: reproducibility and implications for quantitative reconstructions of sea surface temperature variations. Int. J. Earth Sci. 98, 53–66.
Pfeiffer, M., Reuning, L., Zinke, J., Garbe-Schönberg, D., Leupold, M., Dullo, W.C., 2019. 20th century δ18O seawater and salinity variations reconstructed from paired δ18O and Sr/Ca measurements of a La Reunion coral. Paleoceanogr. Paleoclimatol. 34 (12), 2183–2200.
Philander, S., 1990. El Niño, La Niña, and the Southern Oscillation. Academic, San Diego, CA, pp. 293.
Picaut, J., Ioualalen, M., Menkes, C., Delcroix, T., McPhaden, M.J., 1996. Mechanism of the Zonal Displacements of the Pacific Warm Pool: Implications for ENSO. Science 274, 1486–1489.
Qi, J., Zhang, L., Qu, T., Yin, B., Xu, Z., Yang, D., Li, D., Qin, Y., 2019. Salinity variability in the tropical Pacific during the Central-Pacific and Eastern-Pacific El Niño events. J. Mar. Syst. 199, 103225.
Quinn, T.M., Sampson, D.E., 2002. A multiproxy approach to reconstructing sea surface conditions using coral skeleton geochemistry. Paleoceanography 17.
Quinn, T.M., Taylor, F.W., Crowley, T.J., Link, S.M., 1996. Evaluation of sampling resolution in coral stable isotope records: a case study using records from New Caledonia and Tarawa. Paleoceanography 11, 529–542.
Quinn, T.M., Taylor, F.W., Crowley, T.J., 2006. Coral-based climate variability in the Western Pacific Warm Pool since 1867. J. Geophys. Res. Oceans 111.
Ramos, R.D., Goodkin, N.F., Siringan, F.P., Hughen, K.A., 2017. Diploastrea heliopora Sr/Ca and δ18O records from Northeast Luzon, Philippines: An assessment of inter-species coral proxy calibrations and climate controls of sea surface temperature and salinity. Paleoceanography 32, 424–438.
Räsänen, T.A., Lindgren, V., Guillaume, J.H., Buckley, B.M., Kummu, M., 2016. On the spatial and temporal variability of ENSO precipitation and drought teleconnection in mainland Southeast Asia. Clim. Past 12, 1889–1905.
Rasmusson, E.M., Carpenter, T.H., 1982. Variations in tropical sea surface temperature and surface wind fields associated with the Southern Oscillation/El Niño. Mon. Weather Rev. 110, 354–384.
Ren, L., Linsley, B.K., Wellington, G.M., Schrag, D.P., Hoegh-Guldberg, O., 2003. Deconvolving the delta O-18 seawater component from subseasonal coral delta O-18 and Sr/Ca at Rarotonga in the southwestern subtropical Pacific for the period 1726 to 1997. Geochim. Cosmochim. Acta 67, 1609–1621.
Reynolds, R.W., Rayner, N.A., Smith, T.M., Stokes, D.C., Wang, W., 2002. An improved in situ and satellite SST analysis for climate. J. Clim. 15, 1609–1625.
Russon, T., Tudhope, A., Hegerl, G., Collins, M., Tindall, J., 2013. Inter-Annual Tropical Pacific Climate Variability in an Isotope-Enabled CGCM: Implications for Interpreting Coral Stable Oxygen Isotope Records of ENSO.
Sadler, J., Nguyen, A.D., Leonard, N.D., Webb, G.E., Nothdurft, L.D., 2016. Acropora interbranch skeleton Sr/Ca ratios: evaluation of a potential new high-resolution paleothermometer. Paleoceanography 31, 505–517.
Sagar, N., Hetzinger, S., Pfeiffer, M., Masood Ahmad, S., Dullo, W.C., Garbe-Schönberg, D., 2016. High-resolution Sr/Ca ratios in a P orites lutea coral from L akshadweep a rchipelago, southeast arabian Sea: an example from a region experiencing steady rise in the reef temperature. J. Geophys. Res. Oceans 121, 252–266.
Samanta, D., Karnauskas, K.B., Goodkin, N.F., Coats, S., Smerdon, J.E., Zhang, L., 2018. Coupled model biases breed spurious low-frequency variability in the tropical Pacific Ocean. Geophys. Res. Lett. 45, 10,609–610,618.
Samanta, D., Karnauskas, K.B., Goodkin, N.F., 2019. Tropical Pacific SST and ITCZ biases in climate models: double trouble for future rainfall projections? Geophys. Res. Lett. 46, 2242–2252.
Santoso, A., Mcphaden, M.J., Cai, W., 2017. The defining characteristics of ENSO extremes and the strong 2015/2016 El Niño. Rev. Geophys. 55, 1079–1129.
Sayani, H.R., Cobb, K.M., Cohen, A.L., Elliott, W.C., Nurhati, I.S., Dunbar, R.B., Rose, K.A., Zaunbrecher, L.K., 2011. Effects of diagenesis on paleoclimate reconstructions from modern and young fossil corals. Geochim. Cosmochim. Acta 75, 6361–6373.
Sayani, H.R., Cobb, K.M., DeLong, K., Hitt, N.T., Druffel, E.R., 2019. Intercolony δ18O and Sr/Ca variability among Porites spp. corals at Palmyra Atoll: toward more robust coral-based estimates of climate. Geochem. Geophys. Geosyst. 20, 5270–5284.
Schmidt, G.A., Jungclaus, J.H., Ammann, C., Bard, E., Braconnot, P., Crowley, T., Delaygue, G., Joos, F., Krivova, N., Muscheler, R., 2011. Climate Forcing Reconstructions for use in PMIP Simulations of the Last Millennium (v1. 0).
Schollaen, K., Karamperidou, C., Krusic, P., Cook, E., Helle, G., 2015. ENSO flavors in a tree-ring δ18O record of Tectona grandis from Indonesia. Clim. Past 11, 1325–1333.
Schöngart, J., Junk, W.J., Piedade, M.T.F., Ayres, J.M., Hüttermann, A., Worbes, M., 2004. Teleconnection between tree growth in the Amazonian floodplains and the El Nino–Southern Oscillation effect. Glob. Chang. Biol. 10, 683–692.
Schrag, D.P., 1999. Rapid analysis of high-precision Sr/Ca ratios in corals and other marine carbonates. Paleoceanography 14, 97–102.
Shen, C.-C., Lee, T., Chen, C.-Y., Wang, C.-H., Dai, C.-F., Li, L.-A., 1996. The calibration of D [Sr/Ca] versus sea surface temperature relationship for Porites corals. Geochim. Cosmochim. Acta 60, 3849–3858.
Shi, H., Wang, B., 2019. How does the Asian summer precipitation-ENSO relationship change over the past 544 years? Clim. Dyn. 52, 4583–4598.
Singh, A., Delcroix, T., Cravatte, S., 2011. Contrasting the flavors of El Niño-Southern Oscillation using sea surface salinity observations. J. Geophys. Res. Oceans 116.
Smith, S.V., Buddemeier, R.W., Redalje, R.C., Houck, J.E., 1979. Strontium-calcium thermometry in coral skeletons. Science 204, 404–407.
Stahle, D.W., Cook, E.R., Burnette, D.J., Villanueva, J., Cerano, J., Burns, J.N., Griffin, D., Cook, B.I., Acuna, R., Torbenson, M.C., 2016. The Mexican Drought Atlas: tree-ring reconstructions of the soil moisture balance during the late pre-Hispanic, colonial, and modern eras. Quat. Sci. Rev. 149, 34–60.
Stephans, C.L., Quinn, T.M., Taylor, F.W., Corrège, T., 2004. Assessing the reproducibility of coral-bases climate records. Geophys. Res. Lett. 31(L18210, doi:18210.11029/12004GL020343).
Stevenson, S., Powell, B., Merrifield, M., Cobb, K., Nusbaumer, J., Noone, D., 2015. Characterizing seawater oxygen isotopic variability in a regional ocean modeling framework: implications for coral proxy records. Paleoceanography 30, 1573–1593.
Stichler, W., 1995. Interlaboratory comparison of new materials for carbon and oxygen isotope ratio measurements. In: Reference and Intercomparison Materials for Stable Isotopes of Light Elements. 825. pp. 67–74.
Sun, Y., Sun, M., Lee, T., Nie, B., 2005. Influence of seawater Sr content on coral Sr/Ca and Sr thermometry. Coral Reefs 24, 23–29.
Sun, Z., Yang, Y., Zhao, J., Tian, N., Feng, X., 2018. Potential ENSO effects on the oxygen isotope composition of modern speleothems: Observations from Jiguan Cave, Central

China. J. Hydrol. 566, 164–174.
Thirumalai, K., Partin, J.W., Jackson, C.S., Quinn, T.M., 2013. Statistical constraints on El Niño Southern Oscillation reconstructions using individual foraminifera: a sensitivity analysis. Paleoceanography 28, 401–412.
Thompson, L.G., Mosley-Thompson, E., Brecher, H., Davis, M., León, B., Les, D., Lin, P.-N., Mashiotta, T., Mountain, K., 2006. Abrupt tropical climate change: past and present. Proc. Natl. Acad. Sci. 103, 10536–10543.
Thompson, D., Ault, T., Evans, M., Cole, J., Emile-Geay, J., 2011. Comparison of observed and simulated tropical climate trends using a forward model of coral δ 18O. Geophys. Res. Lett. 38.
Timmermann, A., An, S.-I., Kug, J.-S., Jin, F.-F., Cai, W., Capotondi, A., Cobb, K.M., Lengaigne, M., McPhaden, M.J., Stuecker, M.F., 2018. El Niño–southern oscillation complexity. Nature 559, 535–545.
Todd, R.E., Chavez, F.P., Clayton, S., Cravatte, S.E., Goes, M.P., Graco, M.I., Lin, X., Sprintall, J., Zilberman, N.V., Archer, M., 2019. Global perspectives on observing ocean boundary current systems. Front. Mar. Sci. 6, 423.
Trenberth, K.E., 1997. The definition of el nino. Bull. Am. Meteorol. Soc. 78, 2771–2778.
Trenberth, K.E., Stepaniak, D.P., 2001. Indices of el niño evolution. J. Clim. 14, 1697–1701.
Tudhope, A.W., Shimmield, G., Chilcott, C., Jebb, M., Fallick, A., Dalgleish, A., 1995. Recent changes in climate in the far western equatorial Pacific and their relationship to the Southern Oscillation; oxygen isotope records from massive corals, Papua New Guinea. Earth Planet. Sci. Lett. 136, 575–590.
Tudhope, A.W., Chilcott, C.P., McCulloch, M.T., Cook, E.R., Chappell, J., Ellam, R.M., Lea, D.W., Lough, J.M., Shimmield, G.B., 2001. Variability in the El Niño-Southern Oscillation through a glacial-interglacial cycle. Science 291, 1511–1517.
Urey, H.C., 1947. The thermodynamic properties of isotopic substances. J. Chem. Soc. 562–581.
Wallace, J., Rasmusson, E., Mitchell, T., Kousky, V., Sarachik, E., Von Storch, H., 1998. On the structure and evolution of ENSO-related climate variability in the tropical Pacific: Lessons from TOGA. J. Geophys. Res. Oceans 103, 14241–14259.
Wang, X., Liu, H., 2016. Seasonal-to-interannual variability of the barrier layer in the western Pacific warm pool associated with ENSO. Clim. Dyn. 47, 375–392.
Williams, A.P., Funk, C., 2011. A westward extension of the warm pool leads to a westward extension of the Walker circulation, drying eastern Africa. Clim. Dyn. 37, 2417–2435.
Wittenberg, A.T., 2009. Are historical records sufficient to constrain ENSO simulations? Geophys. Res. Lett. 36.
Wu, C.H., Grottoli, A., 2010. Stable oxygen isotope records of corals and a sclerosponge in the Western Pacific warm pool. Coral Reefs 29, 413–418.
Wu, C.H., Linsley, B.K., Dassié, E.P., Schiraldi, B., Demenocal, P.B., 2013. Oceanographic variability in the South Pacific Convergence Zone region over the last 210 years from multi-site coral Sr/Ca records. Geochem. Geophys. Geosyst. 14, 1435–1453.
Wu, C.H., Moreau, M., Linsley, B.K., Schrag, D.P., Corrège, T., 2014. Investigation of sea surface temperature changes from replicated coral Sr/Ca variations in the eastern equatorial Pacific (Clipperton Atoll) since 1874. Palaeogeogr. Palaeoclimatol. Palaeoecol. 412, 208–222.
Wyrtki, K., 1974. Sea level and the seasonal fluctuations of the equatorial currents in the western Pacific Ocean. J. Phys. Oceanogr. 4, 91–103.
Wyrtki, K., 1989. Some thoughts about the west Pacific warm pool. In: Proceedings of the Western Pacific International Meeting and Workshop on TOGA COARE. ORSTOM/Nouméa New Caledonia, pp. 99–109.
Yamoah, K.A., Chabangborn, A., Chawchai, S., Schenk, F., Wohlfarth, B., Smittenberg, R.H., 2016. A 2000-year leaf wax-based hydrogen isotope record from Southeast Asia suggests low frequency ENSO-like teleconnections on a centennial timescale. Quat. Sci. Rev. 148, 44–53.
Yan, Ho, C.-R., Zheng, Q., Klemas, V., 1992. Temperature and size variabilities of the Western Pacific Warm Pool. Science 258, 1643–1645.
Zhao, J., Cheng, H., Yang, Y., Tan, L., Spötl, C., Ning, Y., Zhang, H., Cheng, X., Sun, Z., Li, X., 2019. Reconstructing the Western boundary variability of the Western Pacific Subtropical High over the past 200 years via Chinese cave oxygen isotope records. Clim. Dyn. 52, 3741–3757.
Zinke, J., Pfeiffer, M., Timm, O., Dullo, W.C., Davies, G., 2005. Atmosphere–ocean dynamics in the Western Indian Ocean recorded in corals. Philos. Trans. R. Soc. A Math. Phys. Eng. Sci. 363, 121–142.